Prediction of the excavation damaged zone in Callovo-Oxfordian claystone using coupled second gradient model

F. Collin - **B. Pardoen**

Université de Liège
Argenco Department
Belgium

The nuclear electricity corresponds to 13.4 % of the total amount of the world electricity production in 2008. However, there are some disparities between the countries !

(21% of the total amount in OECD countries, which represent 83% of the world production).

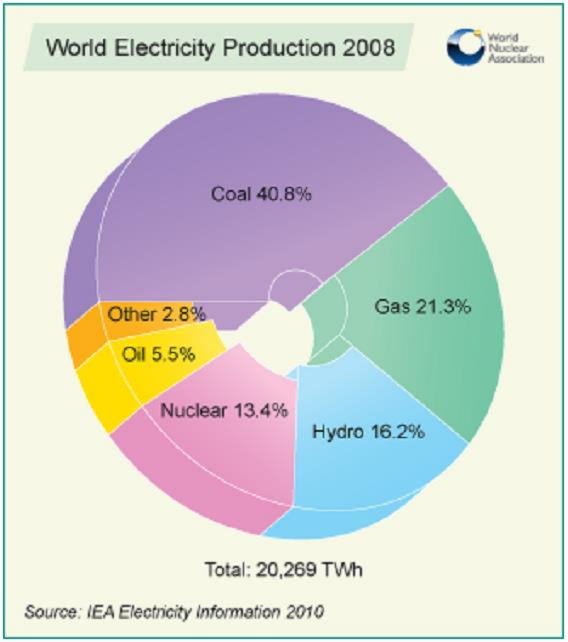

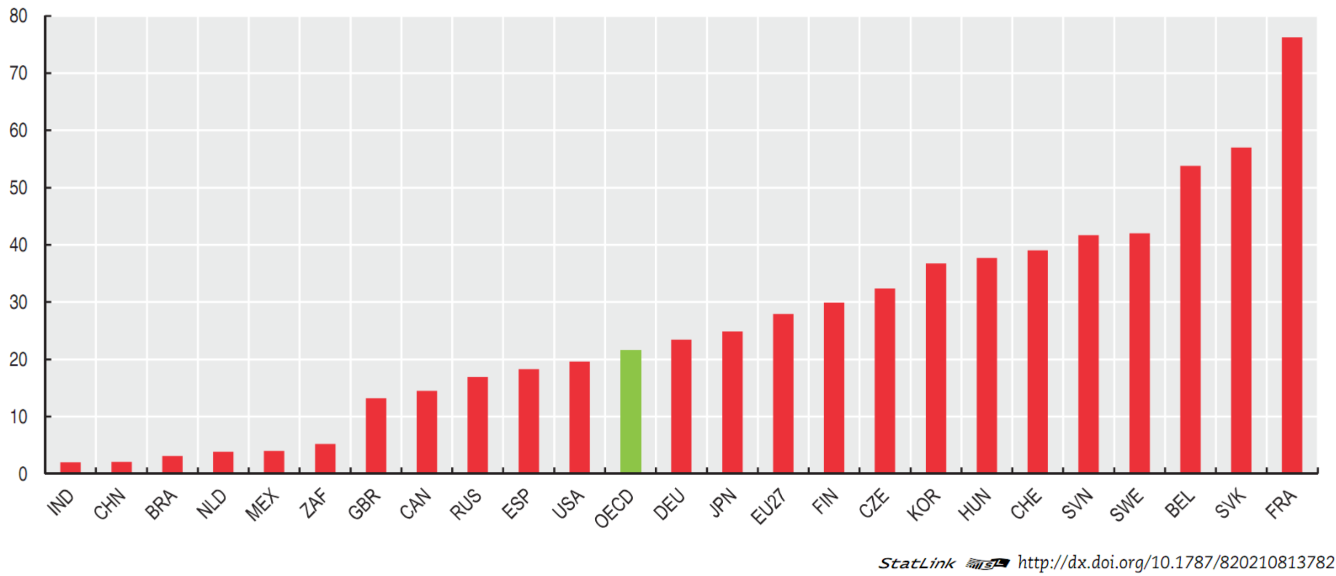

Nuclear electricity generation shares in each country in 2008

Inconvenient

Ionizing radiations

Radioactive waste production

Amount of produced waste

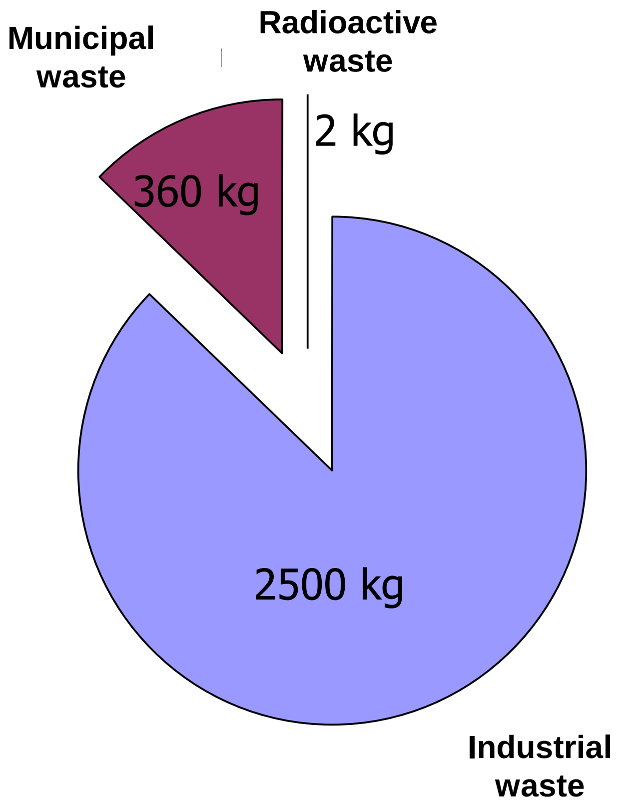

Produced waste in France /year /inhabitant

Source of waste?

- Fuel
- Dismantling
- Protection dress
- …

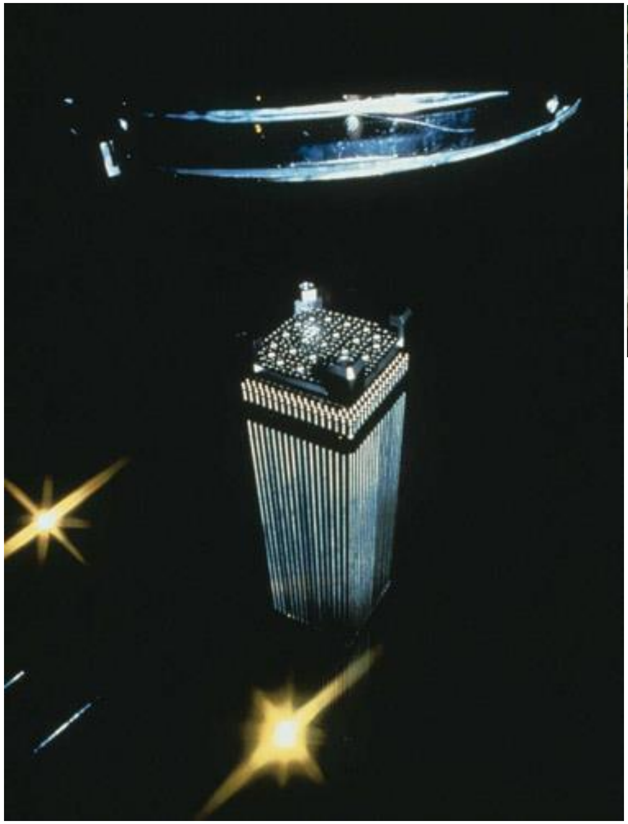

Categories of nuclear wastes

	Short life (< 30 years)	Long life (> 30 years)
Low activity	**Waste A** 90% Volume 1% Radioactivity 70 500 m³ in 2070 in Belgium	
Medium activity		**Waste B** 8% Volume 4% Radioactivity 8900 m³ in 2070 in Belgium
High activity		**Waste C** 2% Volume 95% Radioactivity 3000 m³ in 2070 in Belgium

Introduction: Deep geological disposal

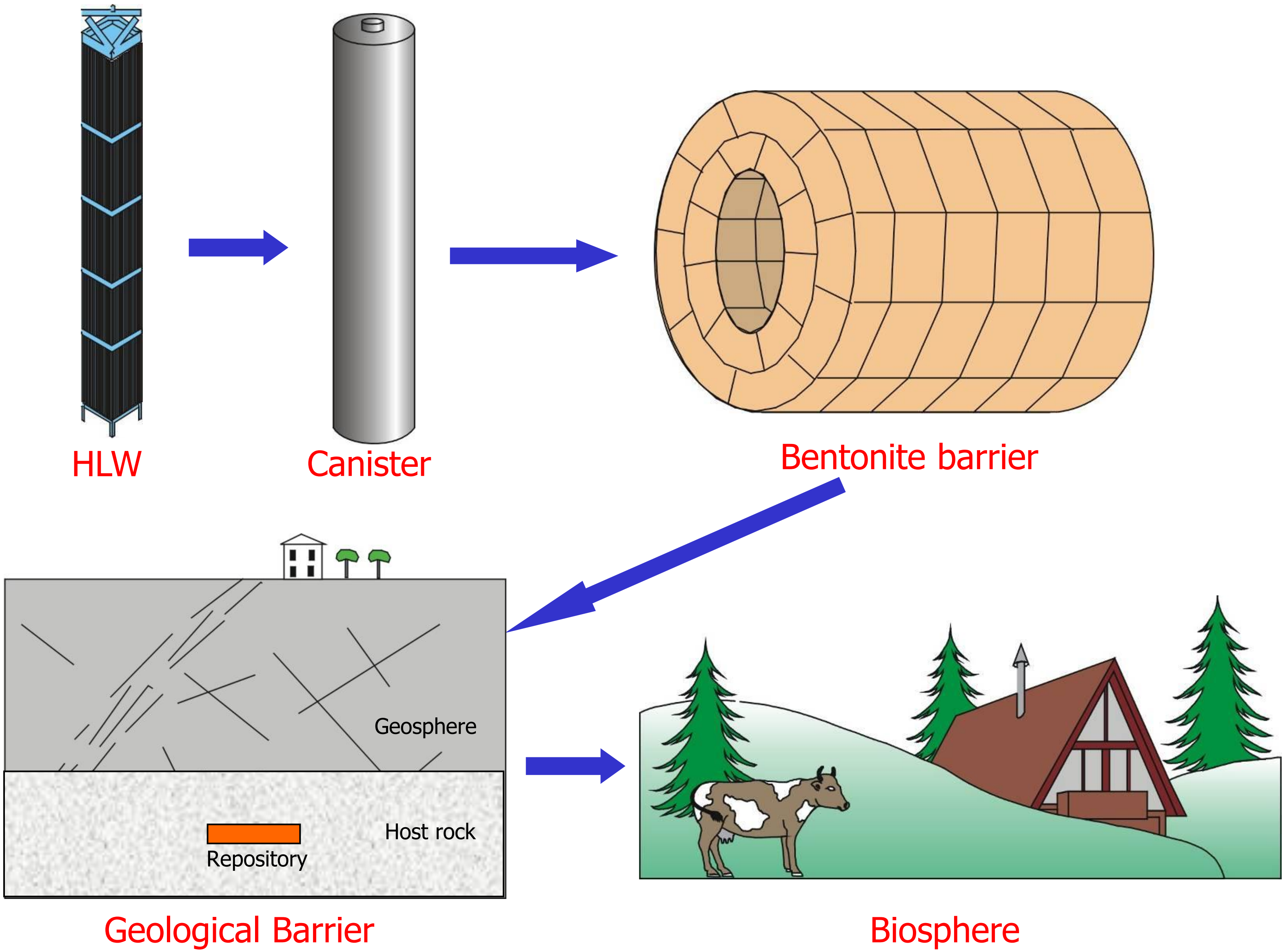

Introduction: Deep geological disposal

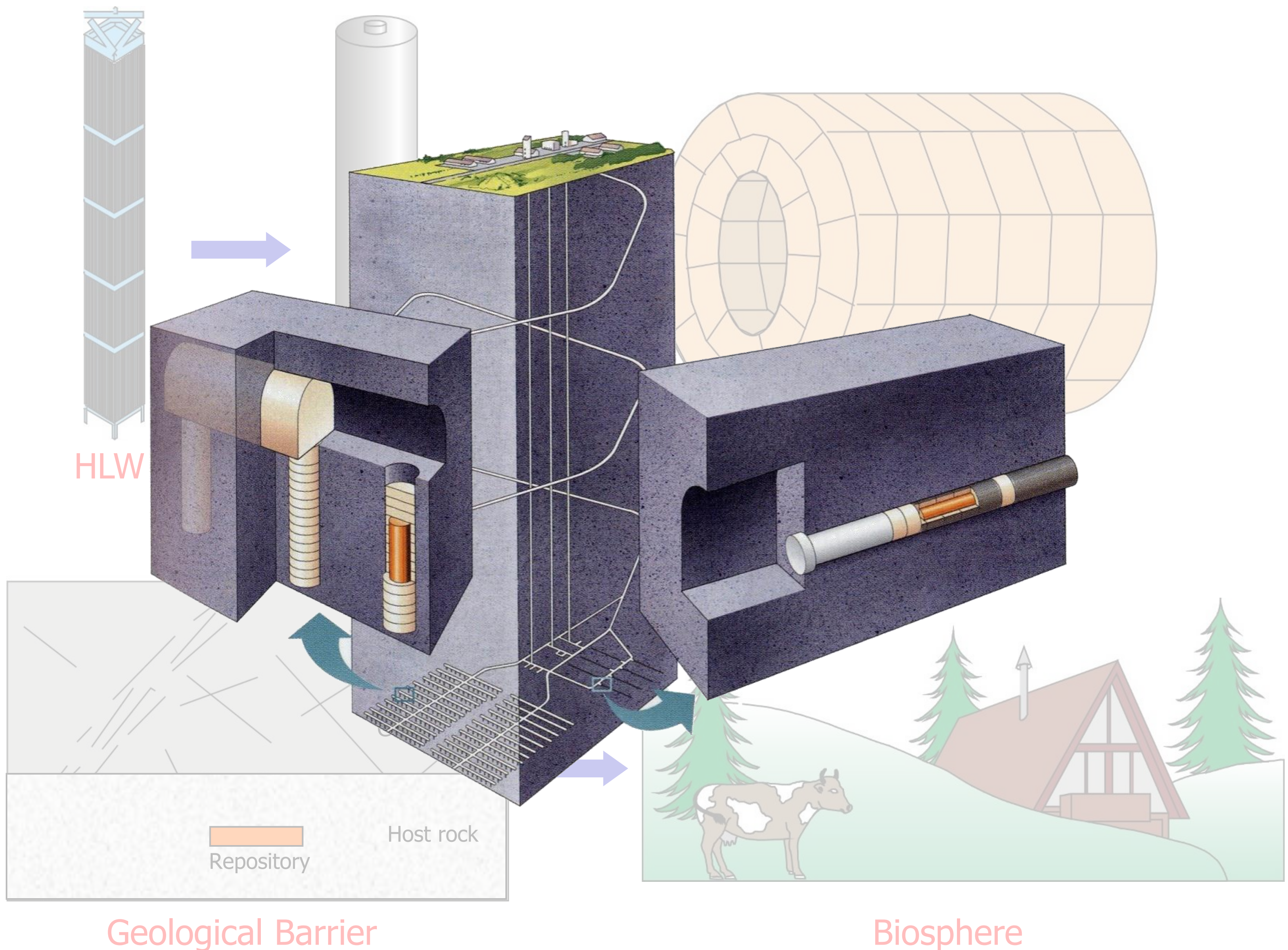

Introduction: Deep geological disposal

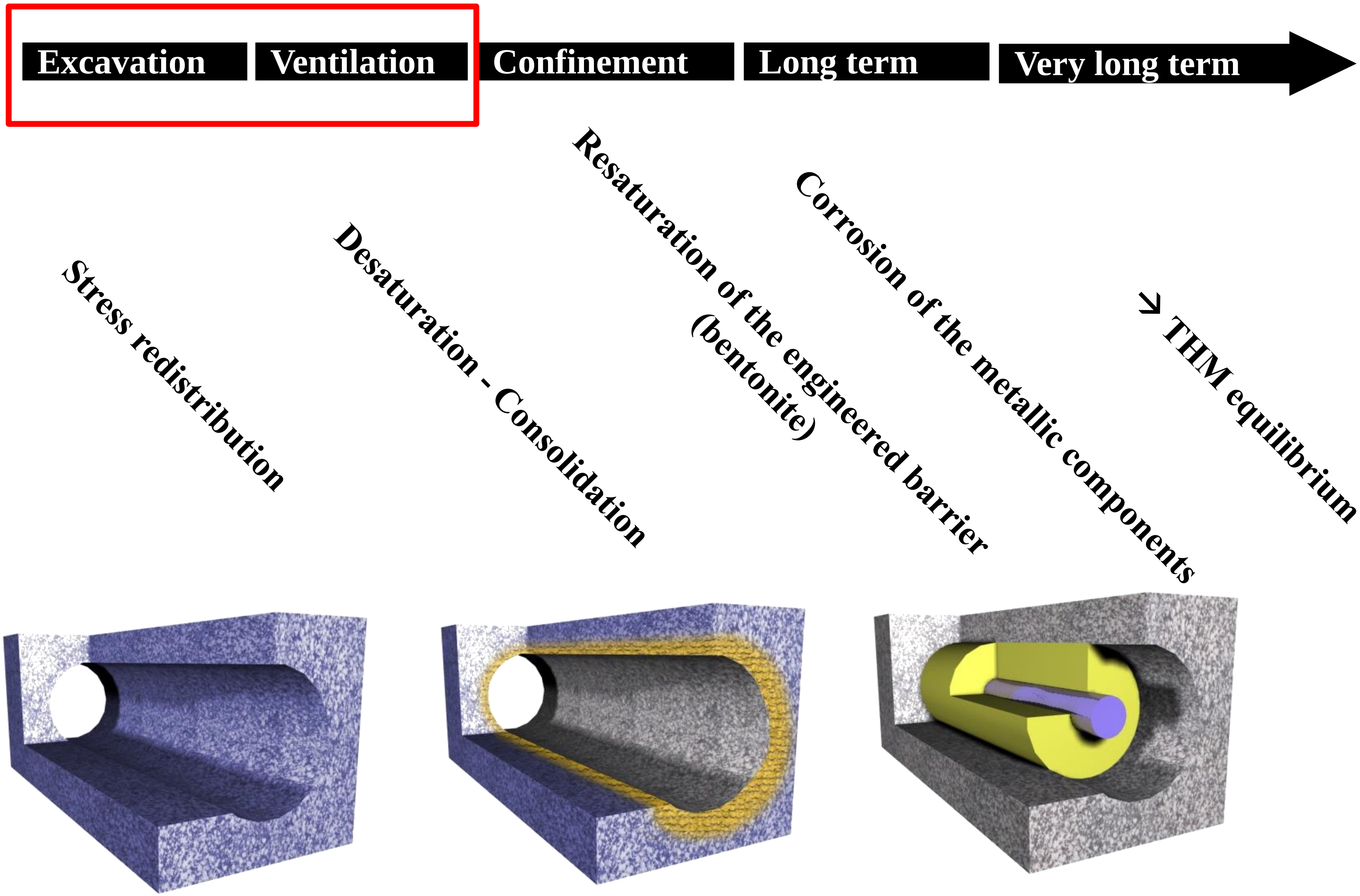

Introduction: Underground research facilities

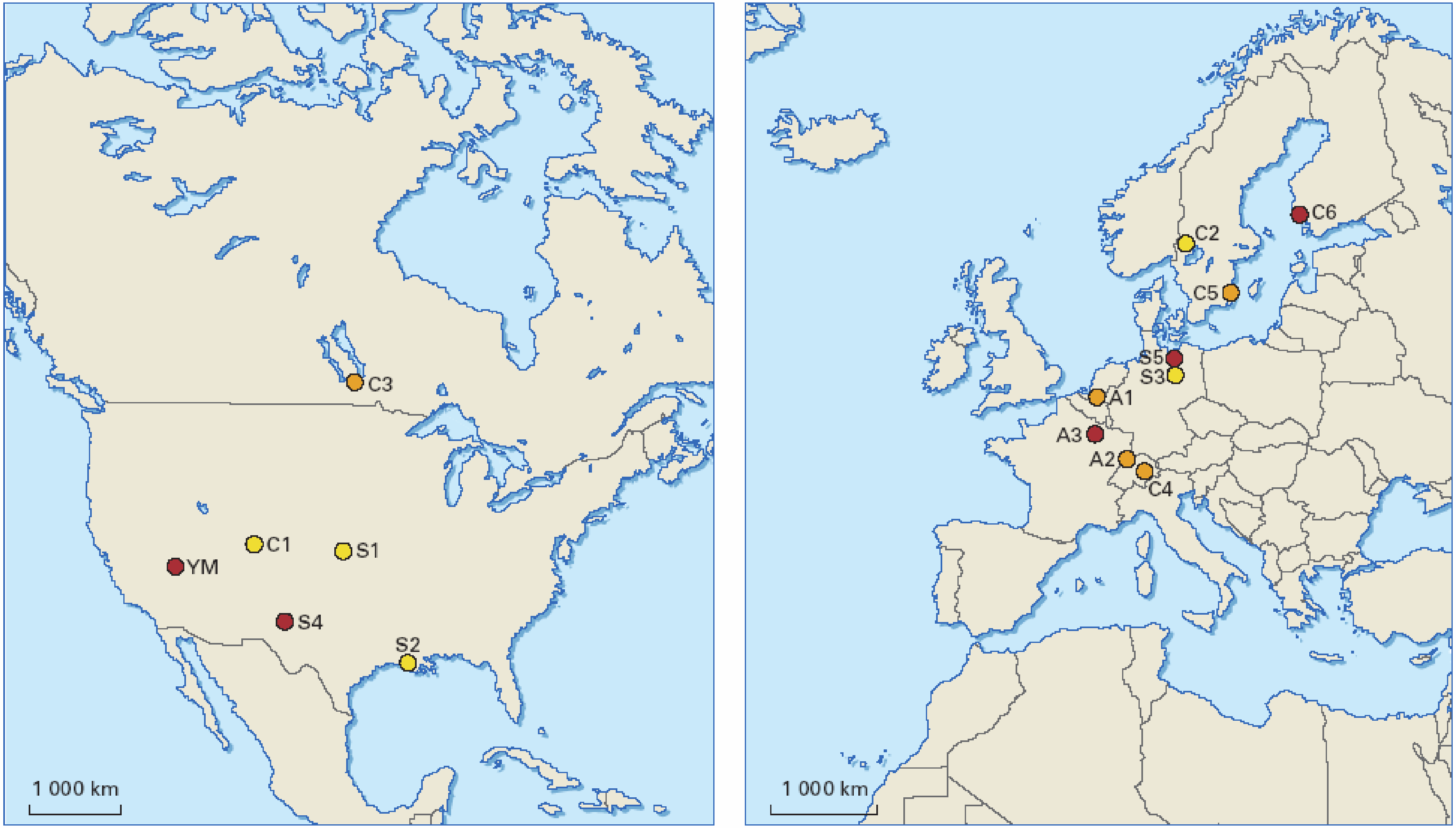

- Mines (expériences 1re génération)
- Laboratoires souterrains génériques
- Laboratoires souterrains de qualification de site

S1 Lyons
S2 Avery Island
S3 Asse
S4 WIPP Carlsbad
S5 Gorleben

C1 Climax
C2 Stripa
C3 Lac du Bonnet
C4 Grimsel
C5 Äspö

C6 Olkiluoto
A1 Mol
A2 Mont Terri
A3 Meuse - Haute-Marne
YM Yucca mountain

Andra – URF at Bure (France):

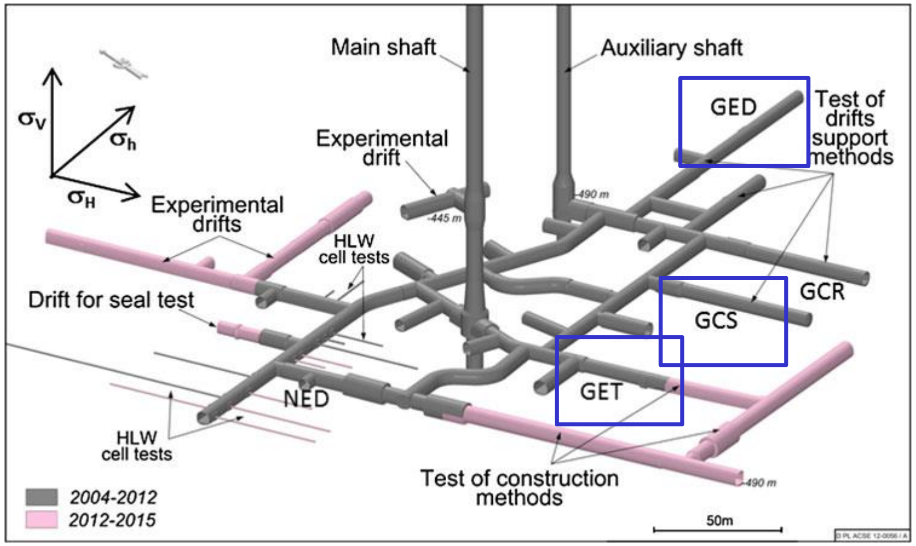

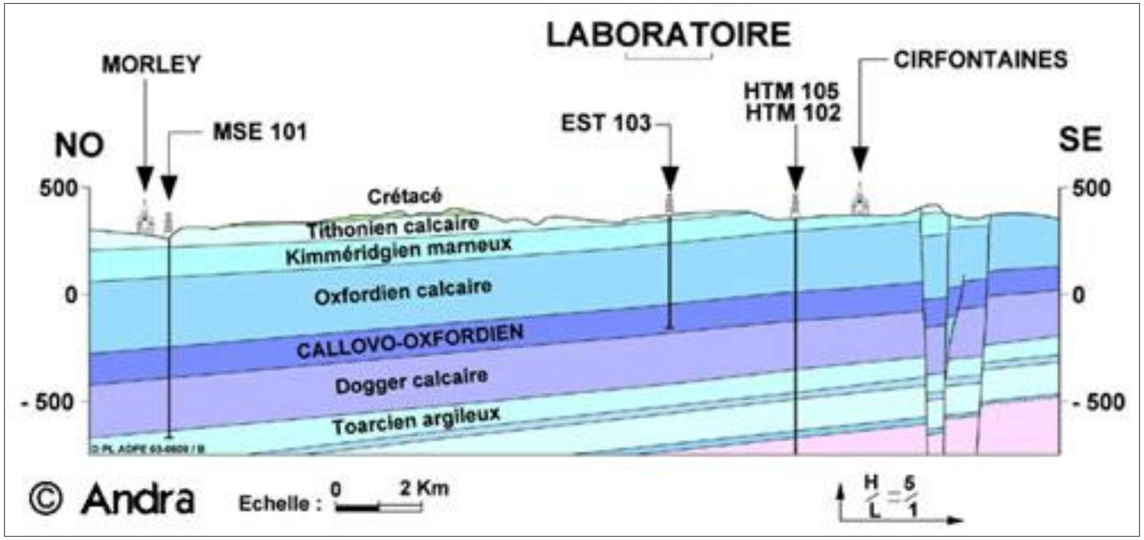

Andra – URF at Bure : In situ experiment

***In situ* evidences (Andra) :** (Armand et al. 2014)

Anisotropy: - stress : $\sigma_H > \sigma_h \sim \sigma_v$
- cross-anisotropy mechanical behaviour
- permeability

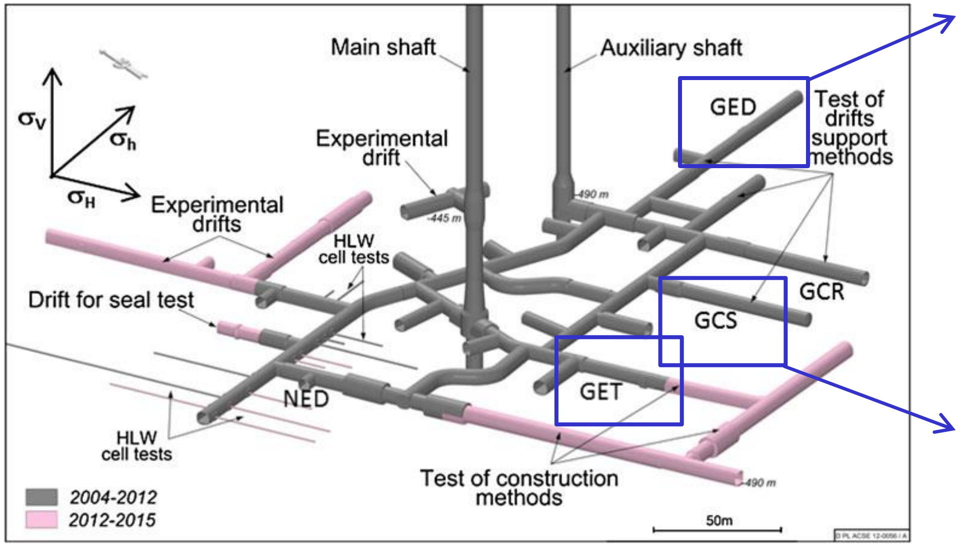

Galery // to σ_h

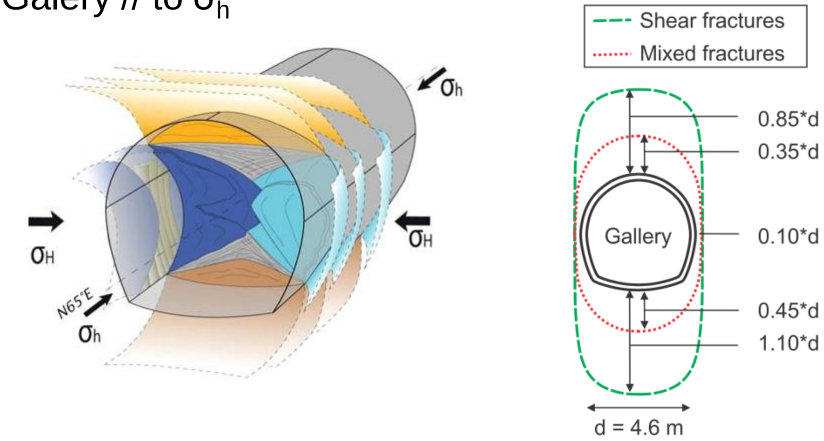

Galery // to σ_H

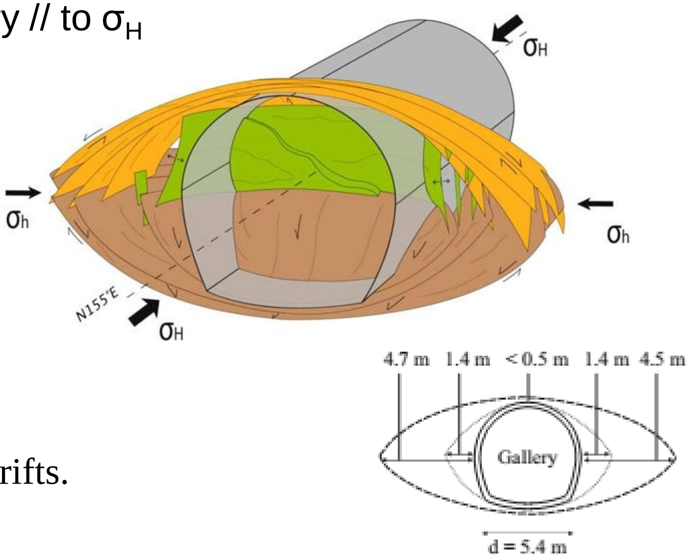

Armand, G. et al. (2014). Geometry and properties of the excavation-induced fractures at the Meuse/Haute-Marne URL drifts. *Rock Mech Rock Eng*, *47*, 21–41.

***In situ* measurement (Andra) :** (Armand et al. 2014)

Convergence + pore pressure

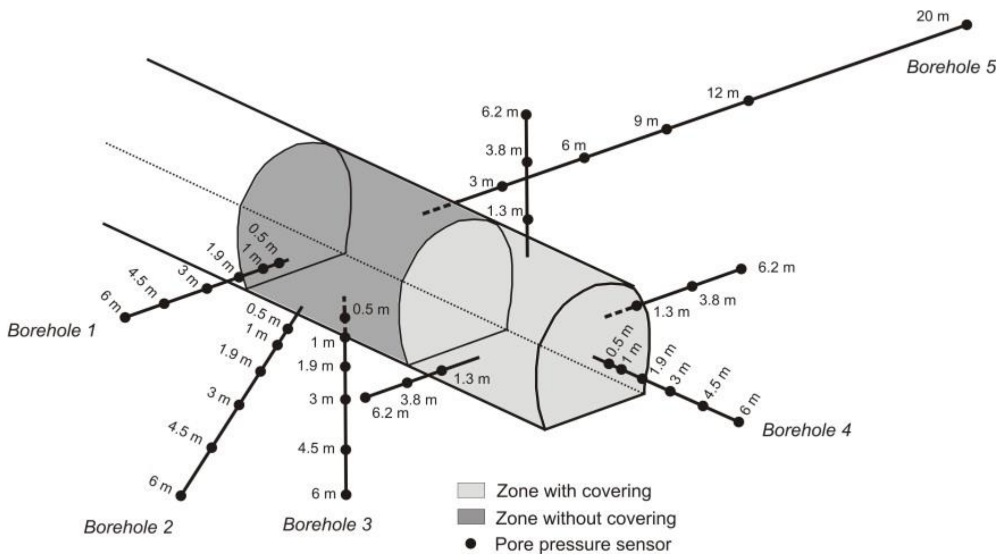

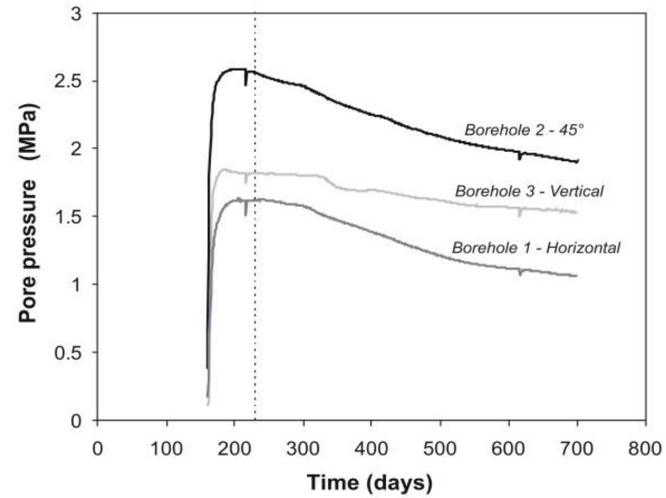

Pore pressure at 4.5 m (SDZ gallery)

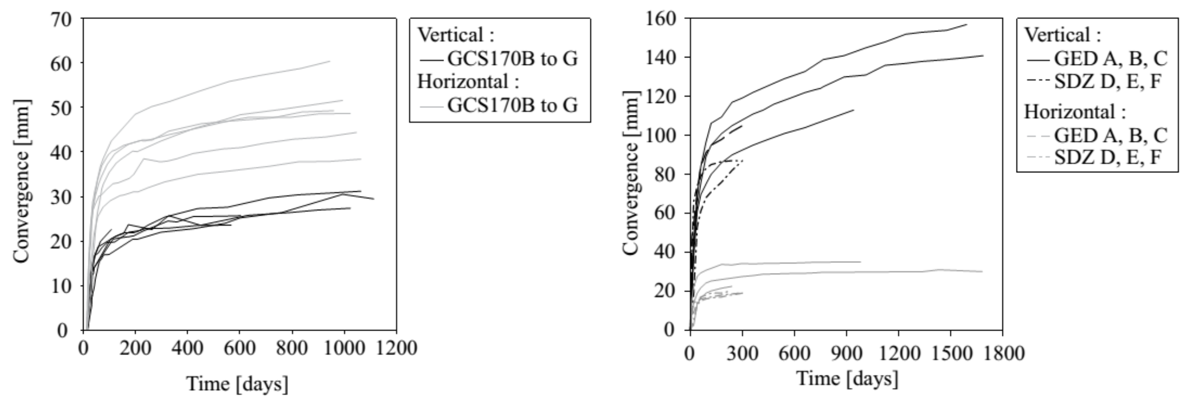

(a) (b)

Observation:

Modification of the mechanical and flow properties within the Excavated damaged zone (EDZ)

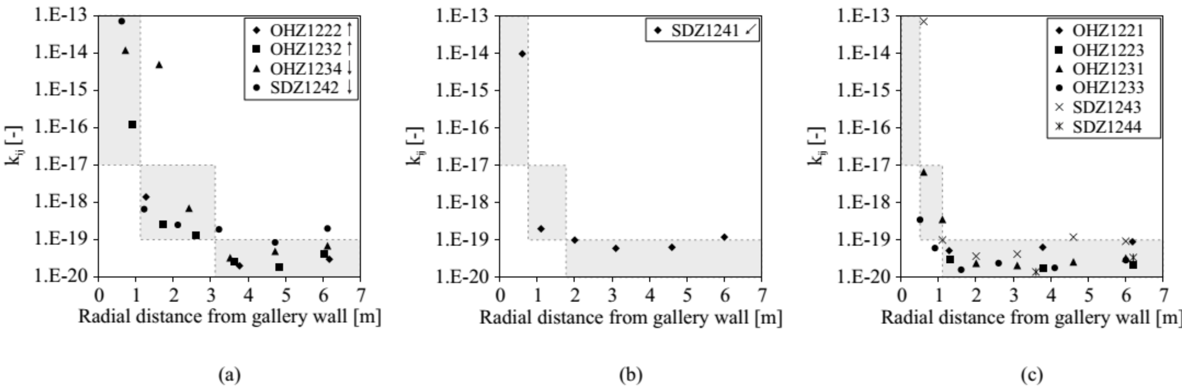

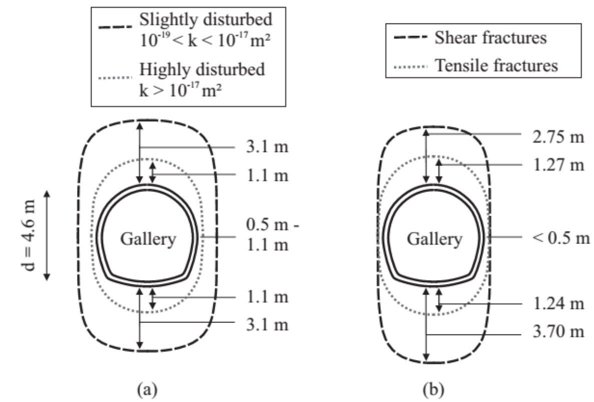

Fig. 2.7: Permeability evolution along (a) vertical, (b) oblique at 45° and (c) horizontal boreholes drilled around a gallery (GED) parallel the minor horizontal principal stress in Callovo-Oxfordian

Numerical challenges:

Major issues : prediction of the extension, fracturing structure and properties modifications.

Study : - fractures modelling with shear strain localisation
- influence of permeability variation

Outline

1. INTRODUCTION

2. SHEAR BAND MODELLING

3. FRACTURES MODELLING

   - GALLERY // TO σ_h

   - GALLERY // TO σ_H

4. PERMEABILITY EVOLUTION

5. CONCLUSION

Shear banding: In situ observation

Shear banding occurs frequently and is the source of many soil and rock engineering problems. In situ observations of shear banding and/or faulting are made frequently at many scales

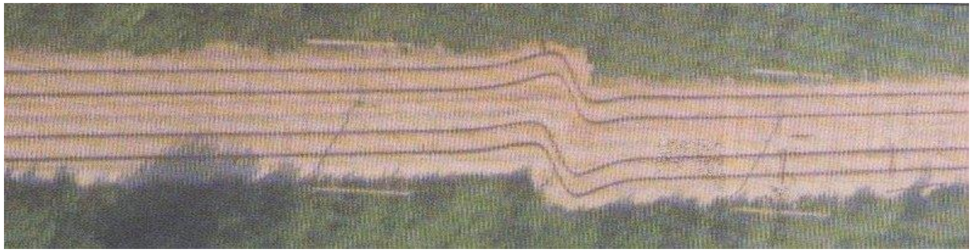

Large scale: railway tracks after an earthquake in Turkey

Triaxial test:

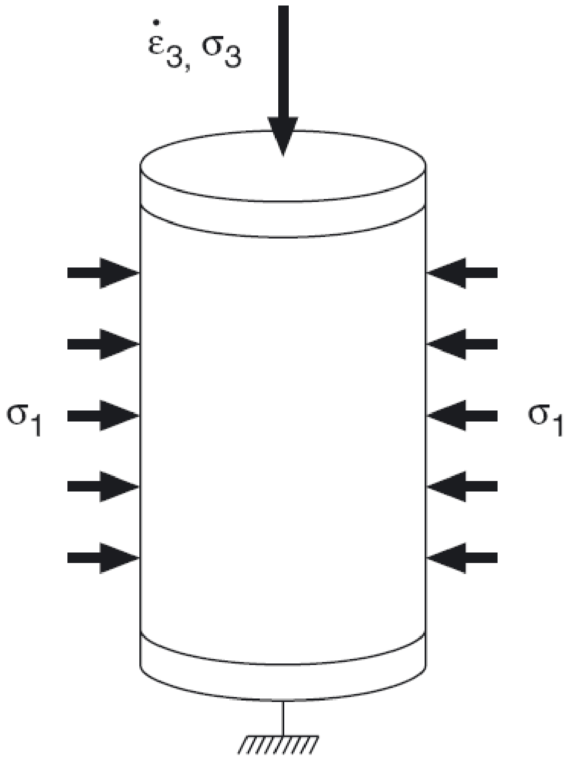

In triaxial tests (and more generally in axi-symmetric tests), the localization zone may remain more or less hidden inside the sample (need for special techniques to see the process)

Shear banding: experimental evidences

Localized rupture in sandstone samples under different confining pressures (Bésuelle et al., 2000)

Experimental characterisation of the localisation phenomenon inside a Vosges sandstone in a triaxial cell
P. BESUELLE, J. DESRUES, S. RAYNAUD, International Journal of Rock Mechanics & Mining Sciences 37 (2000) p. 1223-1237

Shear banding: experimental evidences

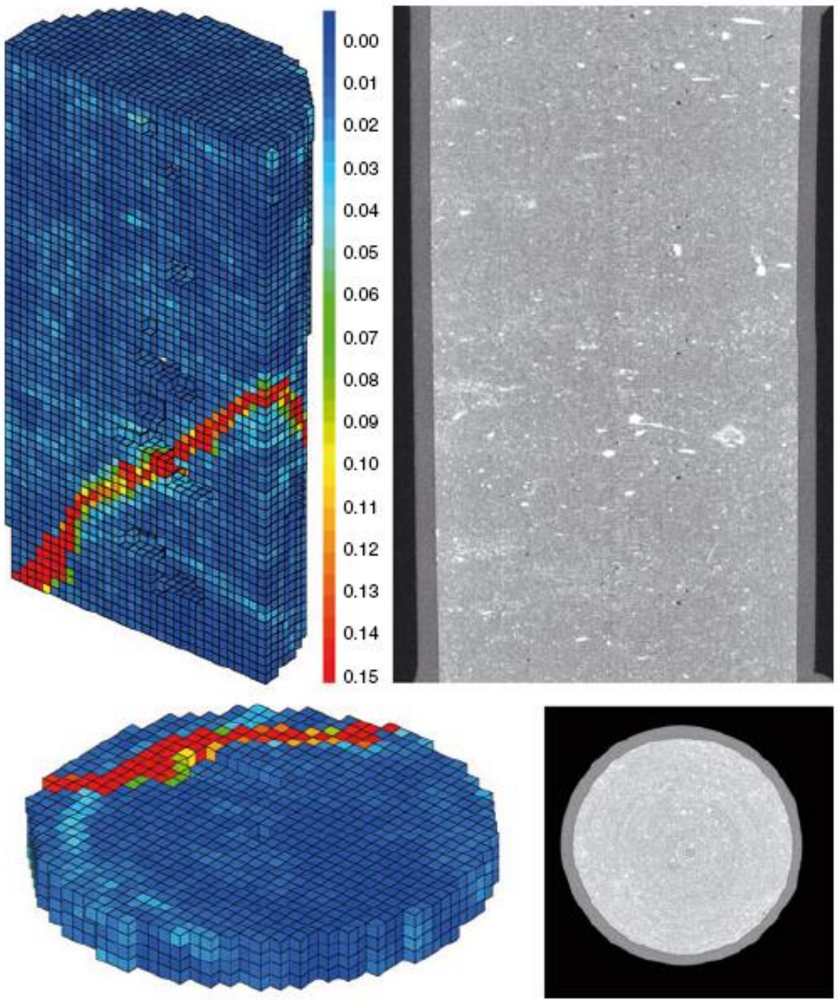

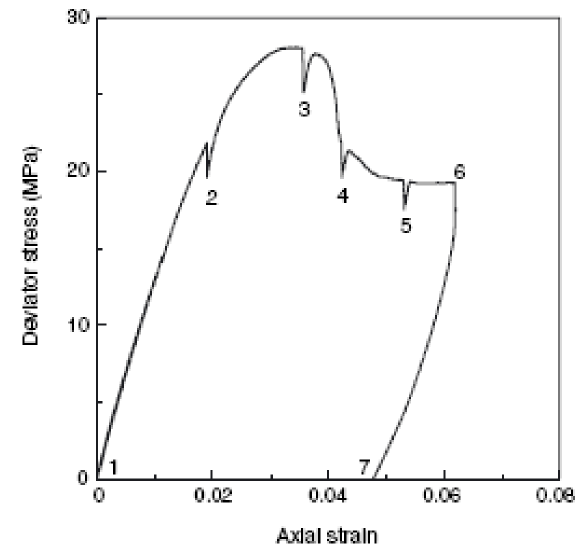

Figure 6: Deviator stress versus axial strain response recorded during test *ESTSYN01* (10 MPa confining stress)

Increment 4-5

3D digital image correlation applied to X-ray micro tomography images from triaxial compression tests on argillaceous rock *LENOIR N , BORNERT M, DESRUES J, BESUELLE P, VIGGIANI G Strain* vol:43 No 3 pp.193-205

Biaxial test:

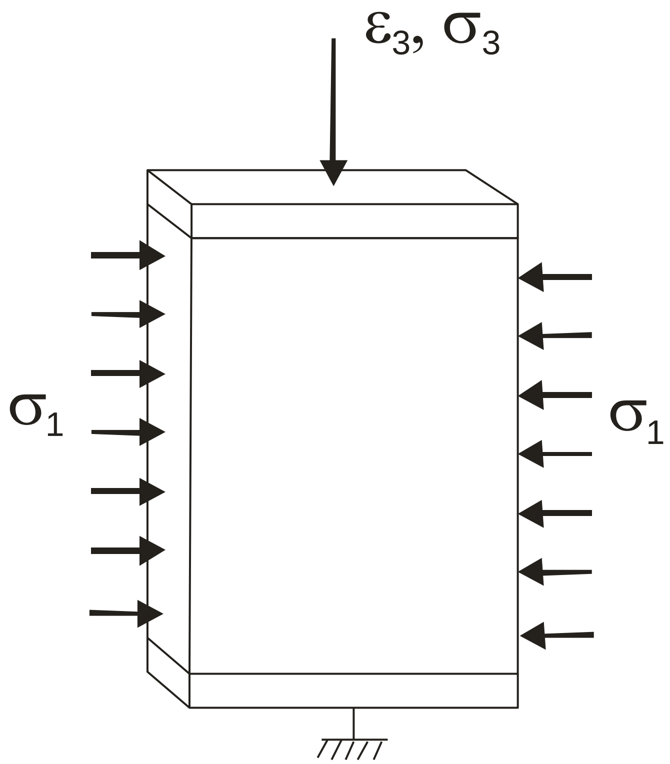

As in triaxial tests (and more generally in axi-symmetric tests), the localization zone may remain more or less hidden inside the sample, most of the experimental campaigns on localization have been performed in biaxial apparatus

Shear banding: experimental evidences

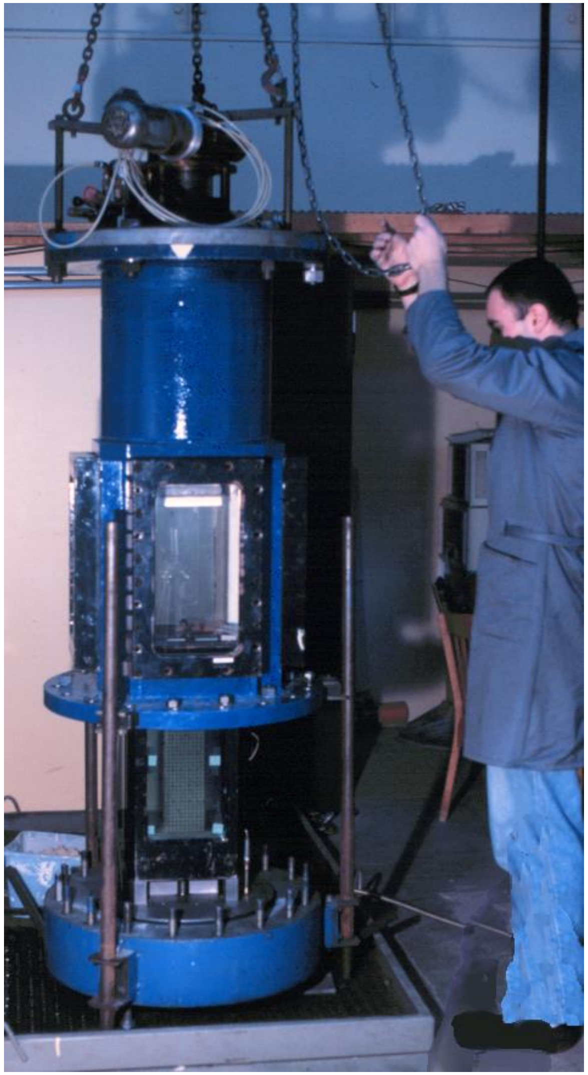

Experimental
set-up
&
a typical test

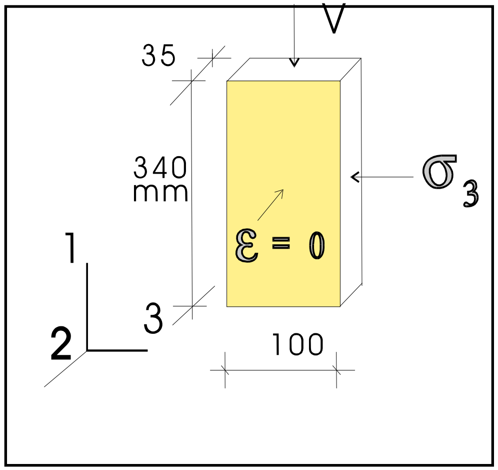

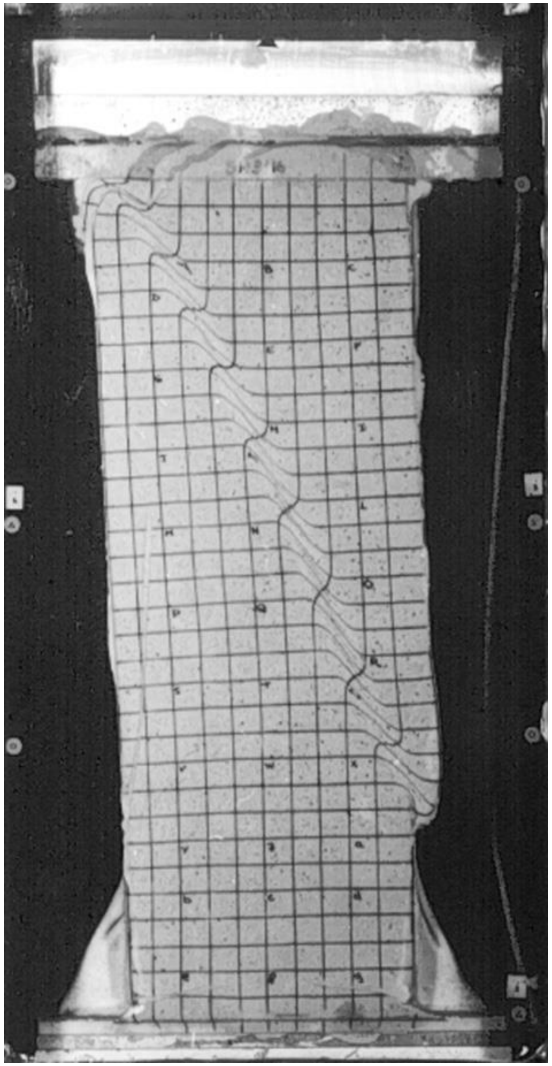

Shear banding: experimental evidences

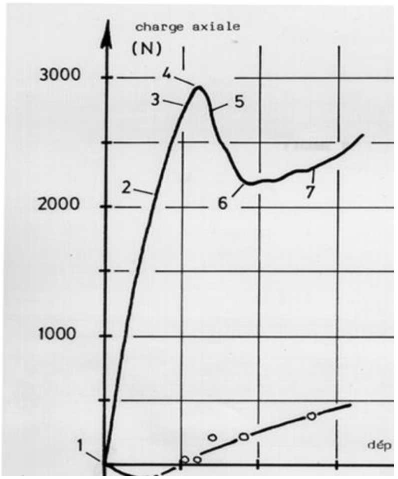

Localization and Peak

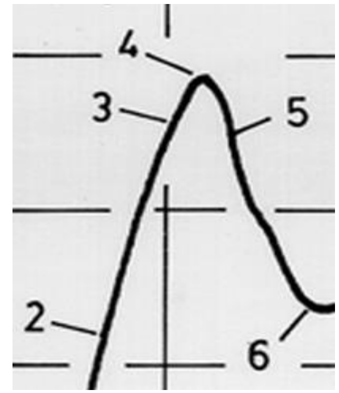

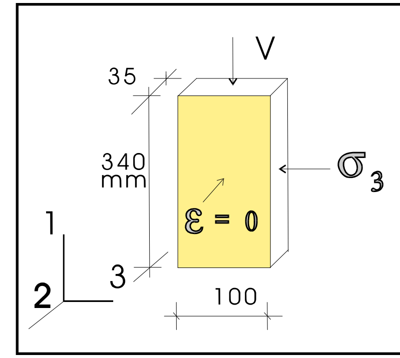

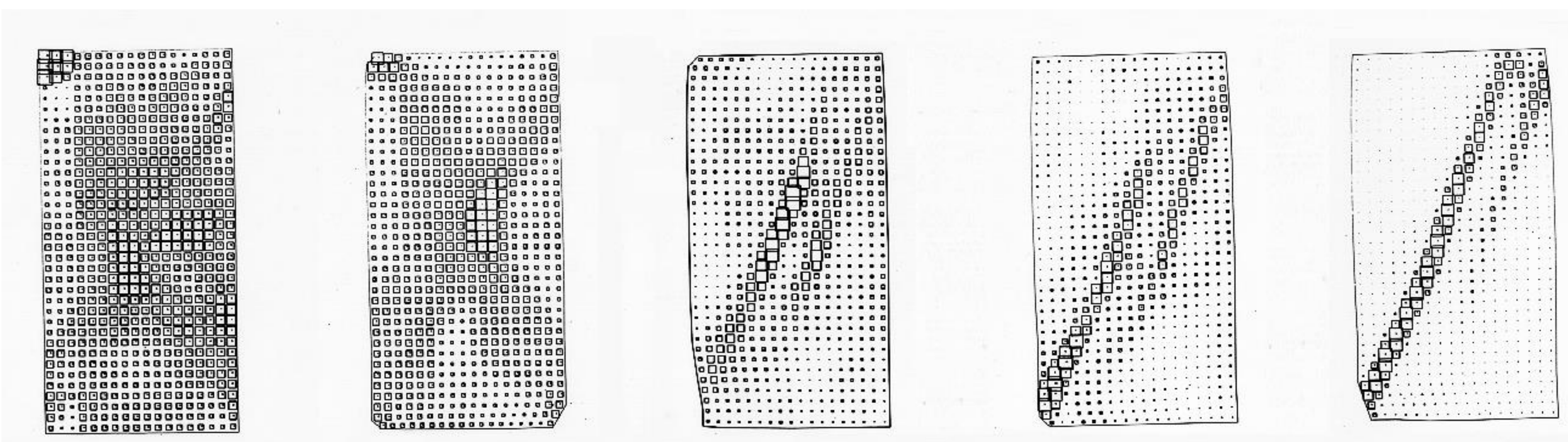

1-2 2-3 3-4 4-5 5-6

Numerical modelling of shear banding

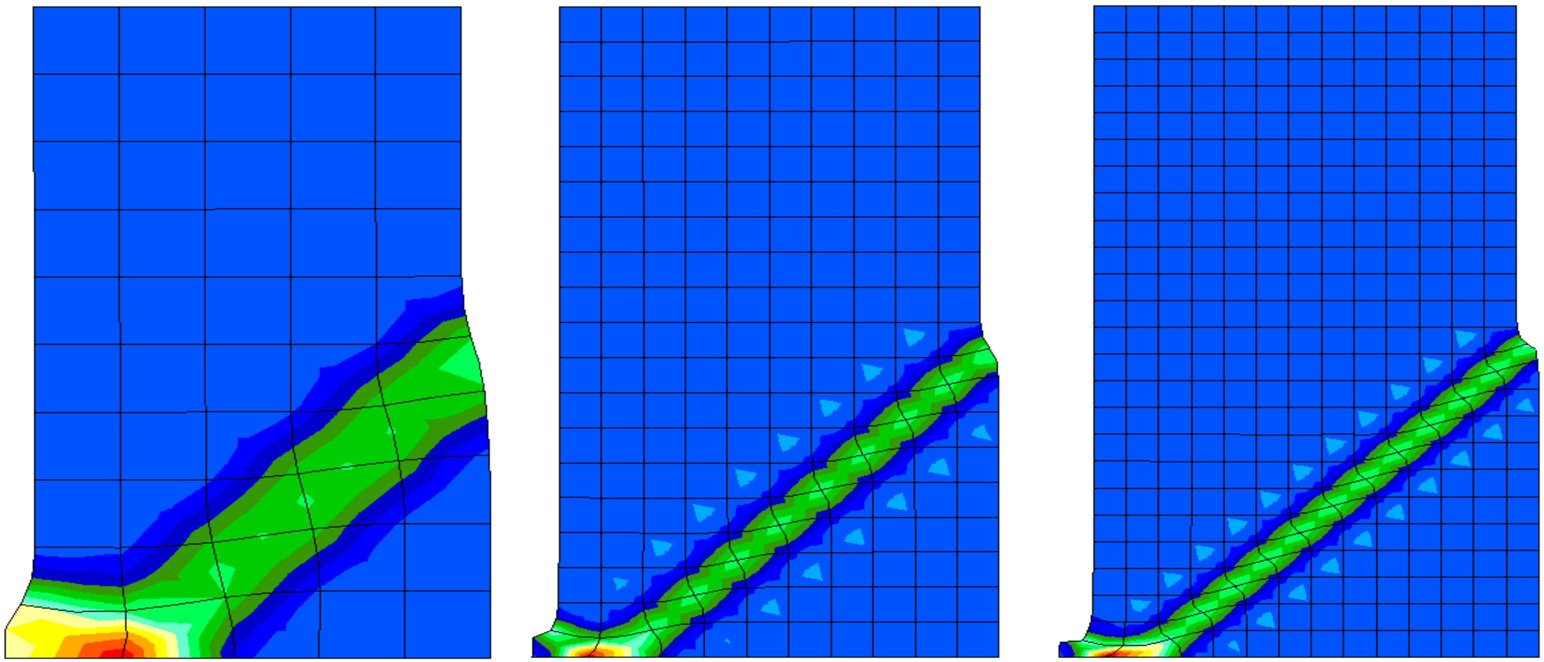

50 elements 200 elements 300 elements

The post peak behaviour depends on the mesh size !

Coupled modelling – Comparison Coarse mesh / Refined mesh

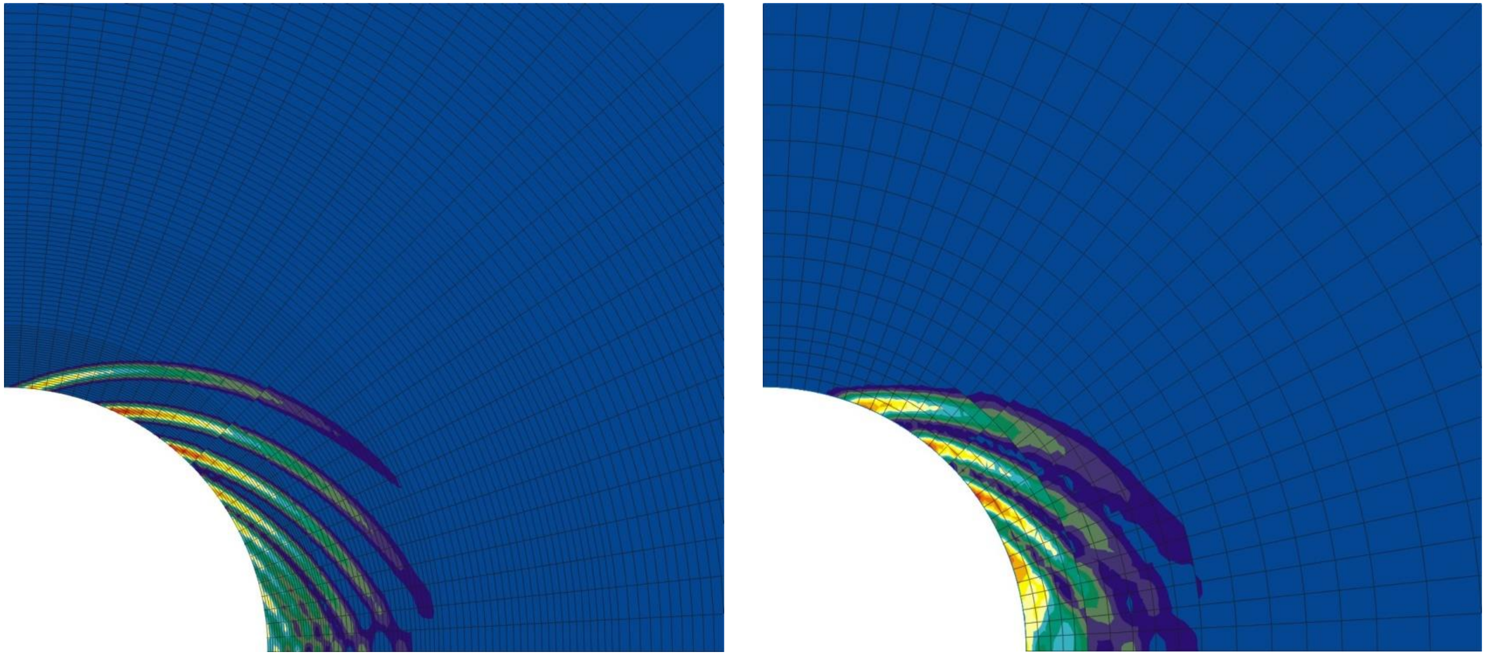

Deviatoric strains

- Classical FE formulation: mesh dependency

- Different regularization methods

Gradient plasticity

Enrichment of the law

Non-local approach

Microstructure continuum

Enrichment of the kinematics

Cosserat model

Second gradient local model

Strain localisation with regularization - Coupled 2^d gradient model : (Chambon *et al.*, 1998 and 2001)

The continuum is enriched with microstructure effects. The kinematics include the classical one (macro) and the microkinematics (Toupin 1962, Mindlin 1964, Germain 1973).

Biphasic porous media : solid + fluid (Collin et al., 2006)

Balance equations for biphasic porous media :

$$\int_{\Omega} \left(\sigma_{ij} \frac{\partial u_i^*}{\partial x_j} + \Sigma_{ijk} \frac{\partial^2 u_i^*}{\partial x_j \partial x_k} \right) d\Omega = \int_{\Omega} G_i u_i^* d\Omega + \int_{\Gamma_\sigma} \left(\bar{t}_i u_i^* + \bar{T}_i D u_i^* \right) d\Gamma$$

$$\int_{\Omega} \left(\frac{\partial M}{\partial t} p_w^* - m_{w,i} \frac{\partial p_w^*}{\partial x_i} \right) d\Omega = \int_{\Omega} Q\, p_w^*\, d\Omega + \int_{\Gamma_q} \bar{q}\, p_w^*\, d\Gamma$$

Effective stress : $\sigma_{ij} = \sigma'_{ij} + b_{ij} S_{rw} p_w$

Double stress : $\tilde{\Sigma}_{ijk} = f\left(B, \frac{\partial^2 u_i^*}{\partial x_j \partial x_k} \right)$

Second gradient model (mechanical analysis)

Modelling of a compression biaxial test (softening plasticity)

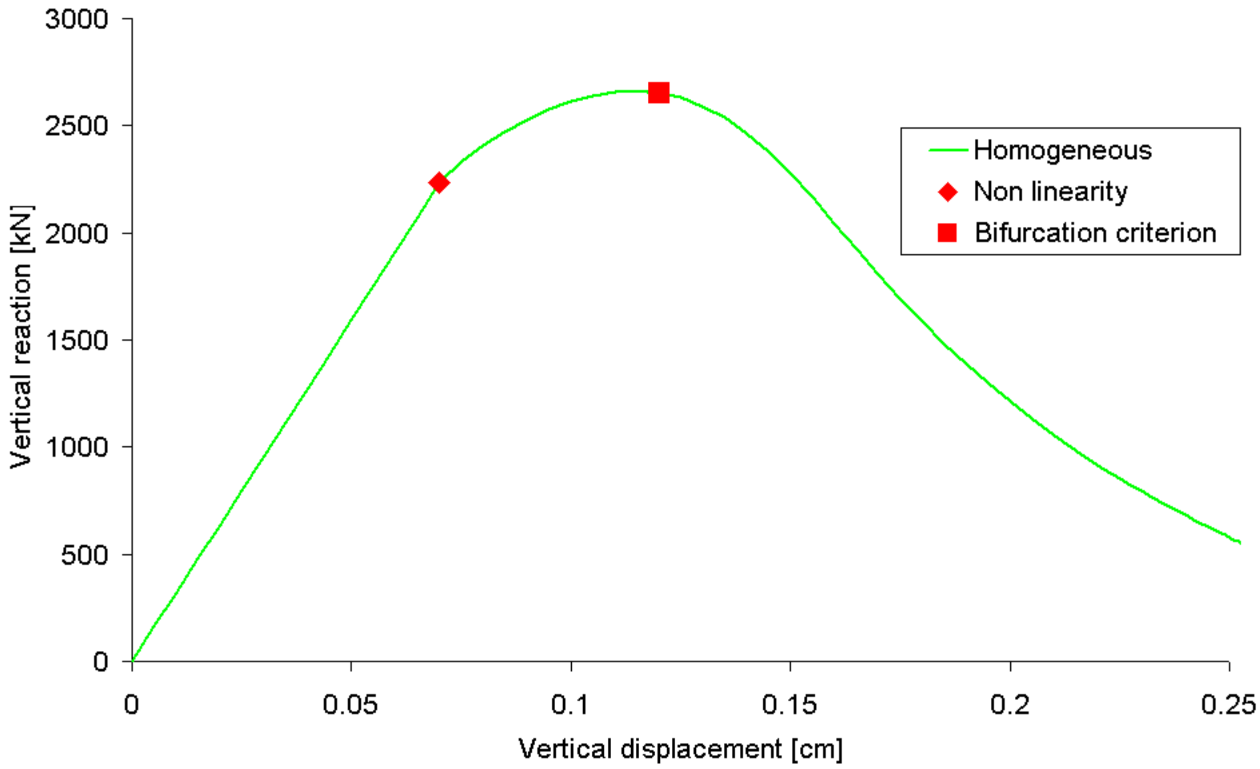

Second gradient model (mechanical analysis)

First modelling: no HM coupling (no overpressure)

Plastic loading point

(Regularization : Second gradient)

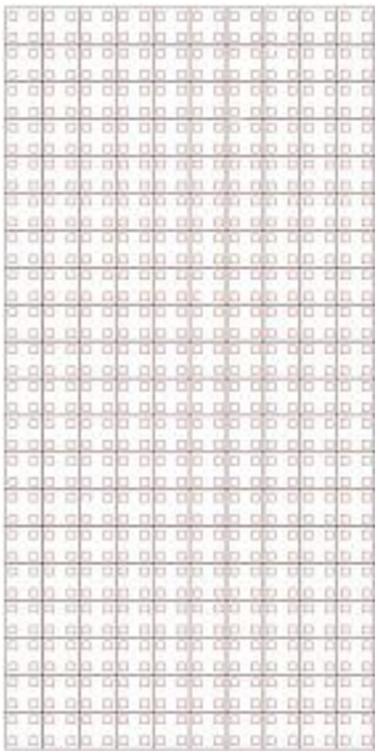

Before

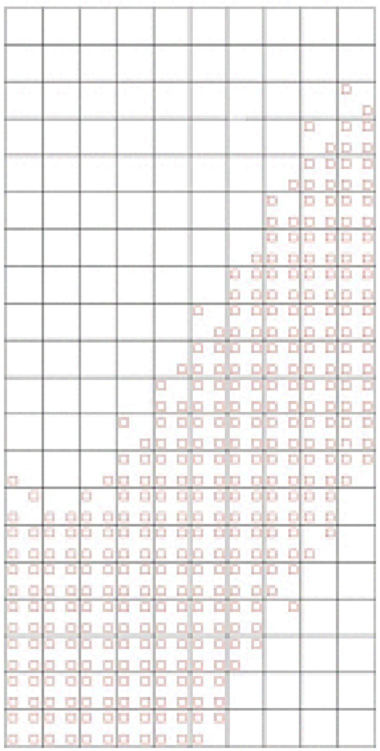

After

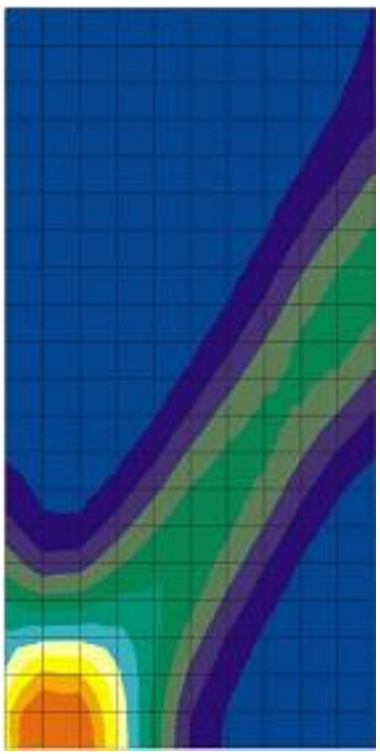

First modelling: no HM coupling (no overpressure)

Velocitiy field

(Regularization : Second gradient)

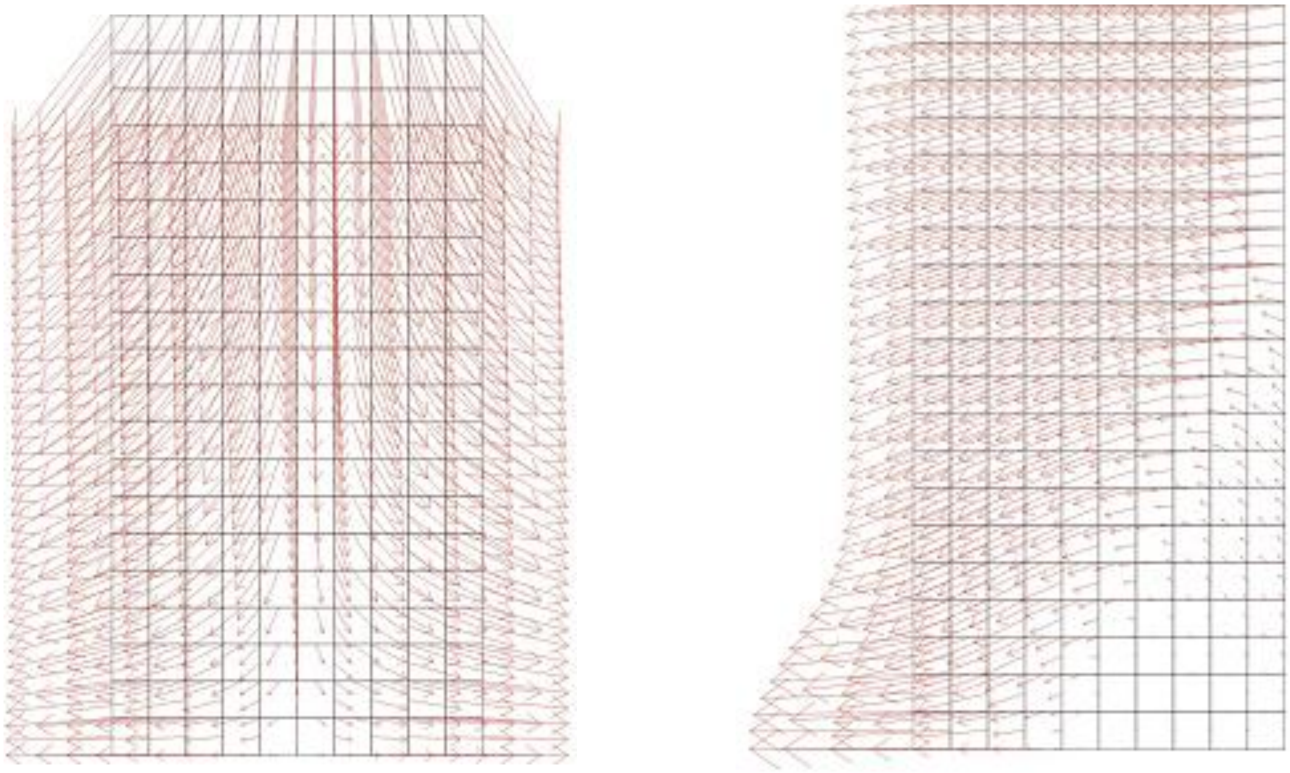

Before *After*

Initiation of localization (Directional research)

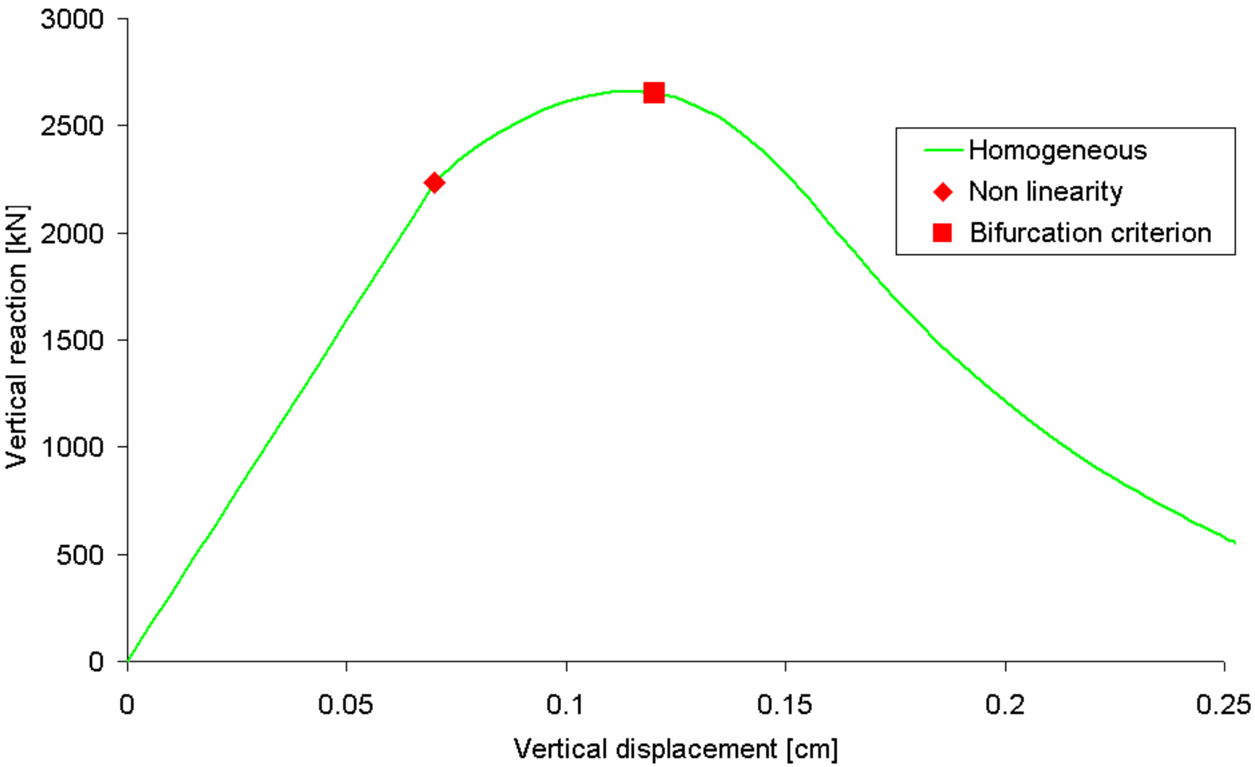

Initiation of localization (Directional research)

(Regularization : Second gradient)

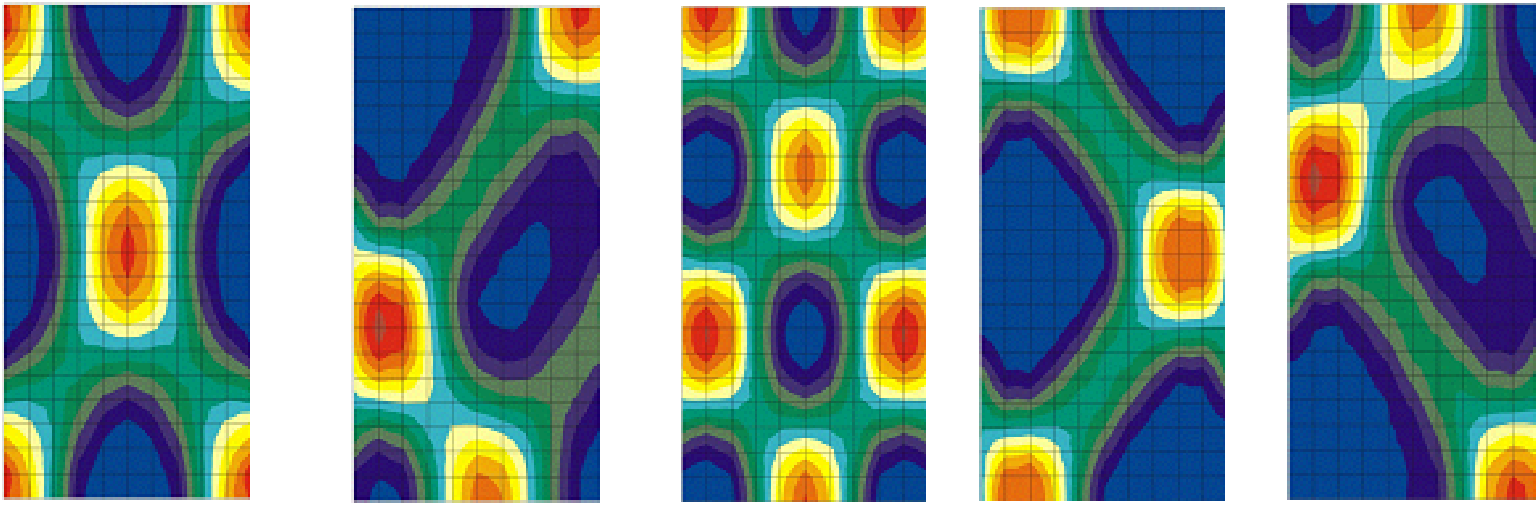

Non uniqueness of the solution

Initiation of localization (Directional research)

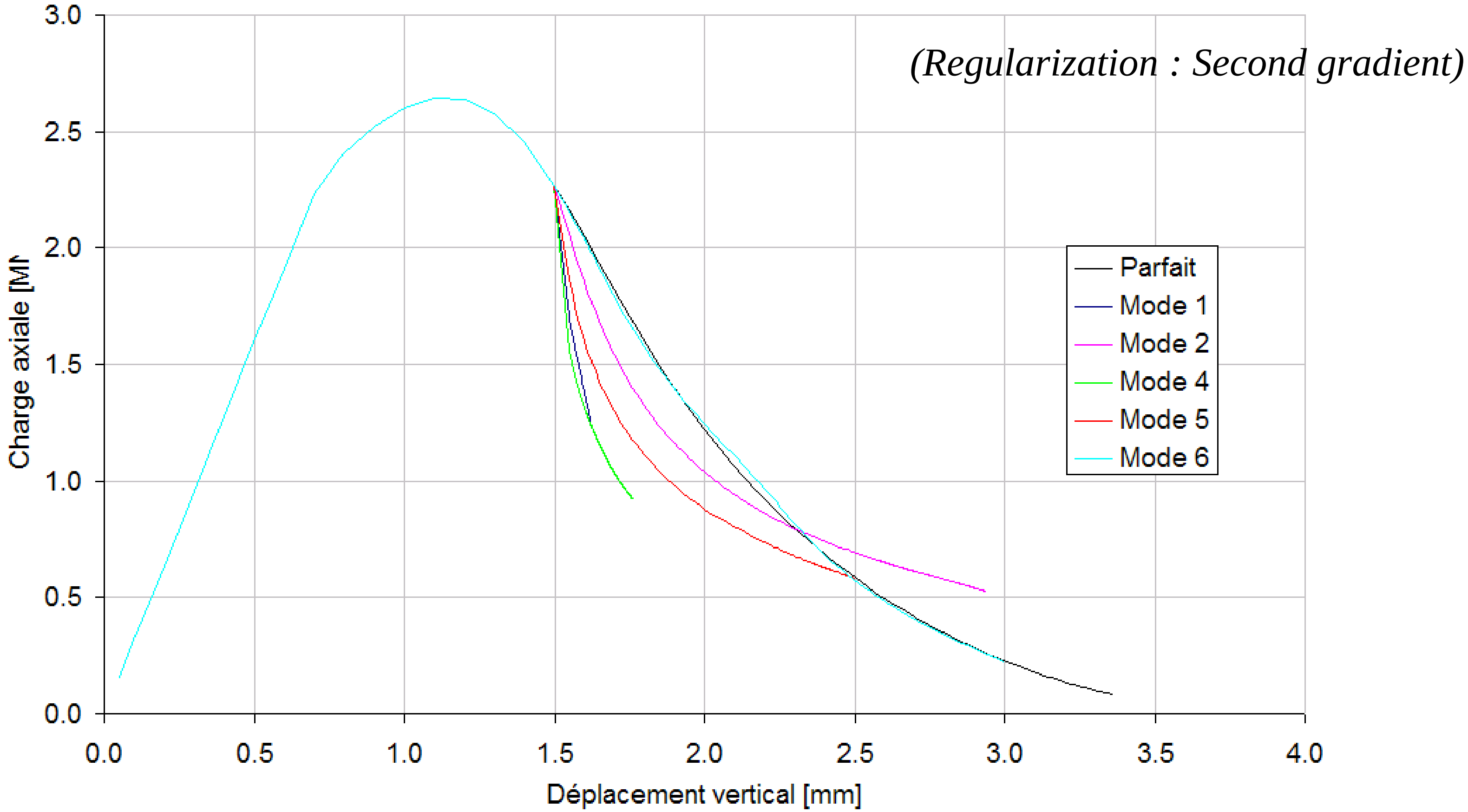

Non uniqueness of the solution

Undrained biaxial compression test

(20 x 10) *(30 x 15)* *(40 x 20)*

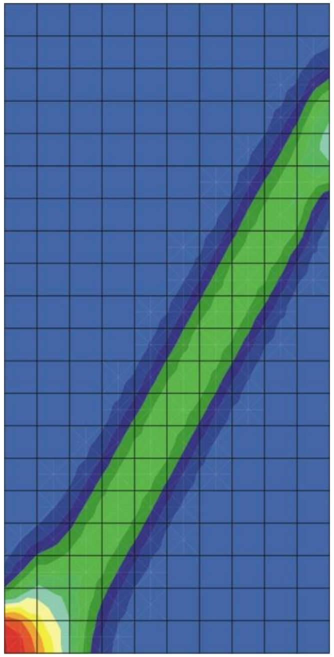

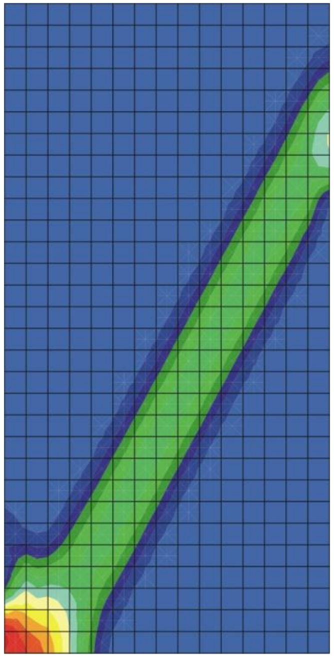

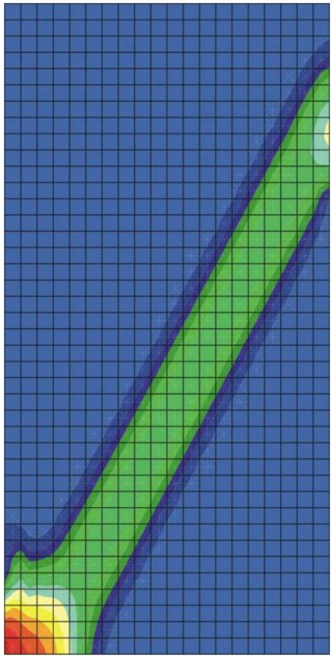

Deviatoric strain

Outline

1. INTRODUCTION
2. SHEAR BAND MODELLING
3. FRACTURES MODELLING
    - GALLERY // TO σ_h
    - GALLERY // TO σ_H
4. PERMEABILITY EVOLUTION
5. CONCLUSION

Mechanical model :

Linear elasticity : Cross-anisotropic (5 param.) + Biot's coefficient

$$d\varepsilon_{ij}^{e} = D_{ijkl}^{e} d\sigma_{kl}^{'} \qquad E_{//}, E_{\perp}, \nu_{////}, \nu_{//\perp}, G_{//\perp}$$

$$b_{ij} = \delta_{ij} - \frac{C_{ijkk}^{e}}{3K_s} \qquad b_{ij} = \begin{bmatrix} b_{//} & & \\ & b_{//} & \\ & & b_{\perp} \end{bmatrix}$$

$$D_{ijkl}^{e} = \begin{bmatrix} \frac{1}{E_{//}} & -\frac{\nu_{////}}{E_{//}} & -\frac{\nu_{\perp//}}{E_{\perp}} & & & \\ -\frac{\nu_{////}}{E_{//}} & \frac{1}{E_{//}} & -\frac{\nu_{\perp//}}{E_{\perp}} & & & \\ -\frac{\nu_{//\perp}}{E_{//}} & -\frac{\nu_{//\perp}}{E_{//}} & \frac{1}{E_{\perp}} & & & \\ & & & \frac{1+\nu_{////}}{E_{//}} & & \\ & & & & \frac{1}{2G_{//\perp}} & \\ & & & & & \frac{1}{2G_{//\perp}} \end{bmatrix}$$

Plasticity :

Van Eeckelen yield surface

Hardening/softening of φ/c :

$$F \equiv II_{\hat{\sigma}} - m\left(I_{\sigma'} + \frac{3c}{\tan\phi_C}\right) = 0$$

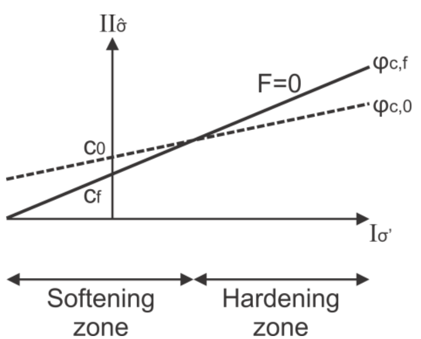

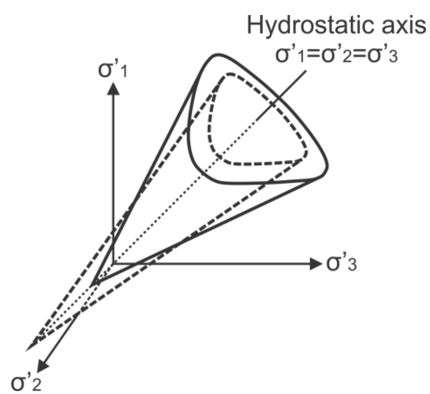

Cohesion anisotropy :

$$c = a_{ij} l_i l_j = \bar{c}\left(1 + A_{11}(1-3l_3^2) + b_1 A_{11}^2 (1-3l_3^2)^2 + \ldots\right)$$

$$l_i = \sqrt{\frac{\sigma_{i1}^{'2} + \sigma_{i2}^{'2} + \sigma_{i3}^{'2}}{\sigma_{ij}^{'}\sigma_{ij}^{'}}}$$

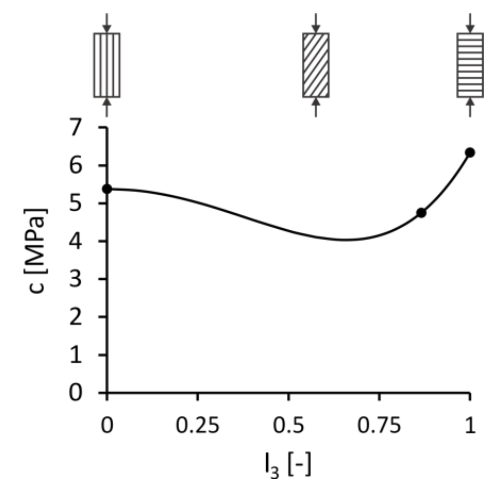

Flow model :

Advection of liquid phase (Darcy's flow) :

$$m_{w,i} = -\rho_w \frac{k_{ij}\, k_{r,w}}{\mu_w} \frac{\partial p_w}{\partial x_j}$$

Water retention and permeability curves (Van Genuchten's model) :

$$S_{r,w} = S_{res} + \left(S_{\max} - S_{res}\right)\left[1 + \left(\frac{p_c}{P_r}\right)^n\right]^{-m}$$

$$k_{r,w} = \sqrt{S_{r,w}}\left[1 - \left(1 - S_{r,w}^{1/m}\right)^m\right]^2$$

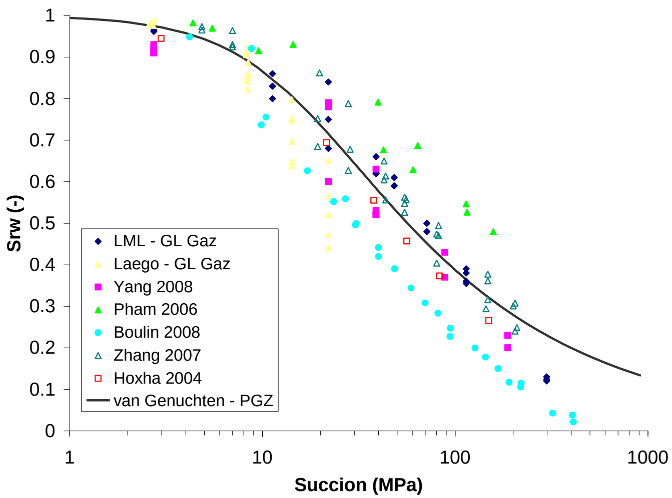

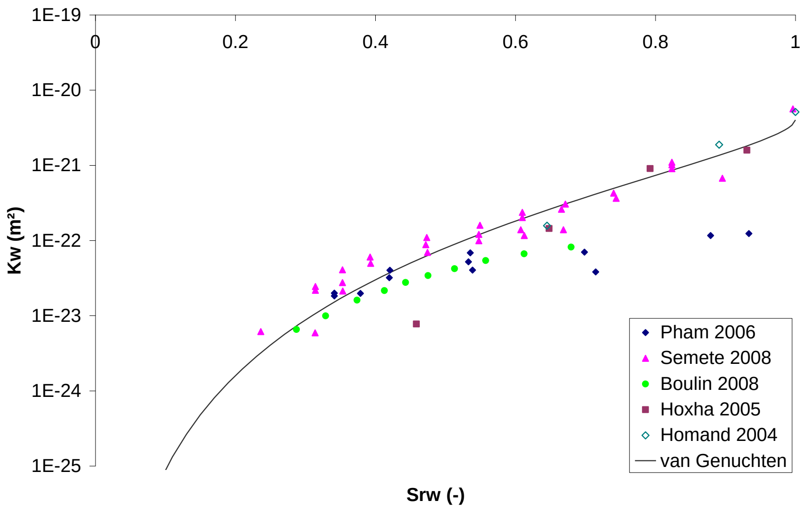

Modelling the EDZ structure

Gallery // to σ_h :

Initial anisotropic stress state(Andra URL) :

$p_{w,0}$ = 4.5 [MPa]
$\sigma_{v,0} = \sigma_{h,0}$ = 12 [MPa]
$\sigma_{H,0}$ = 1.3 $\sigma_{v,0}$ = 15.6 [MPa]

HM modelling in 2D plane strain state (LAGAMINE-Ulg)

Excavation :

$$\sigma_r^\Gamma = (1-\lambda)\sigma_{r,0}^\Gamma$$
$$p_w^\Gamma = (1-\lambda_w)p_{w,0}^\Gamma$$

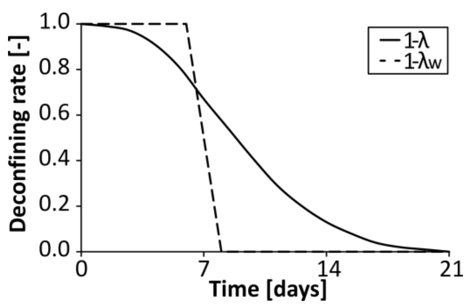

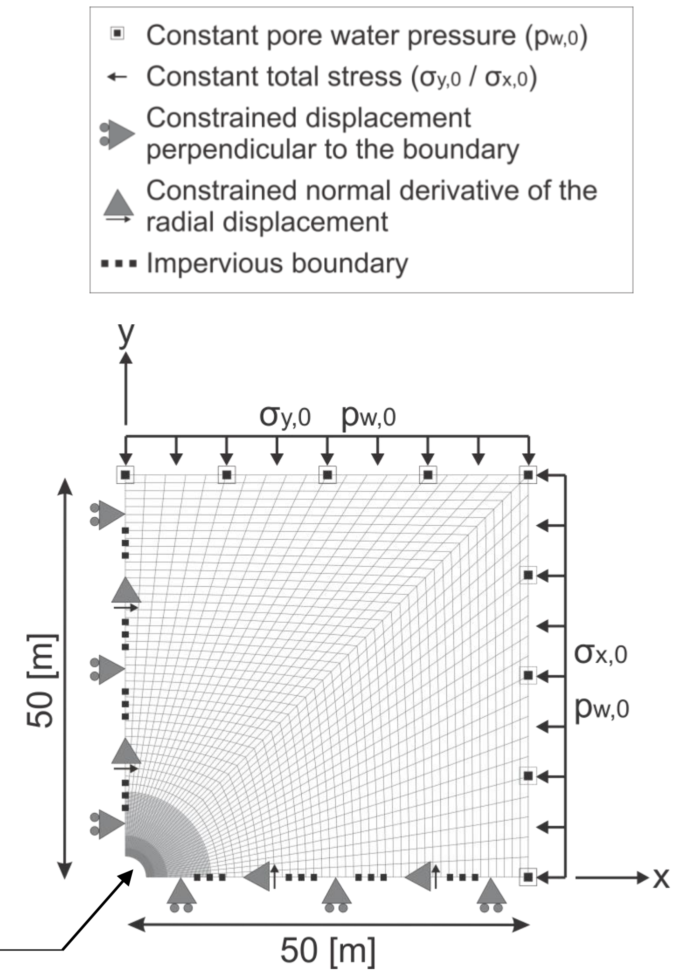

Gallery // to σ_h :

1. Anisotropic stress state + Isotropic model

End of excavation ↓

$\sigma/\sigma_0=0.4$ | $\sigma/\sigma_0=0.2$ | $\sigma/\sigma_0=0.0$

Total deviatoric strain

$$\varepsilon_{eq} = \sqrt{\frac{2}{3}\hat{\varepsilon}_{ij}\hat{\varepsilon}_{ij}}$$

0 0.184

Plasticity

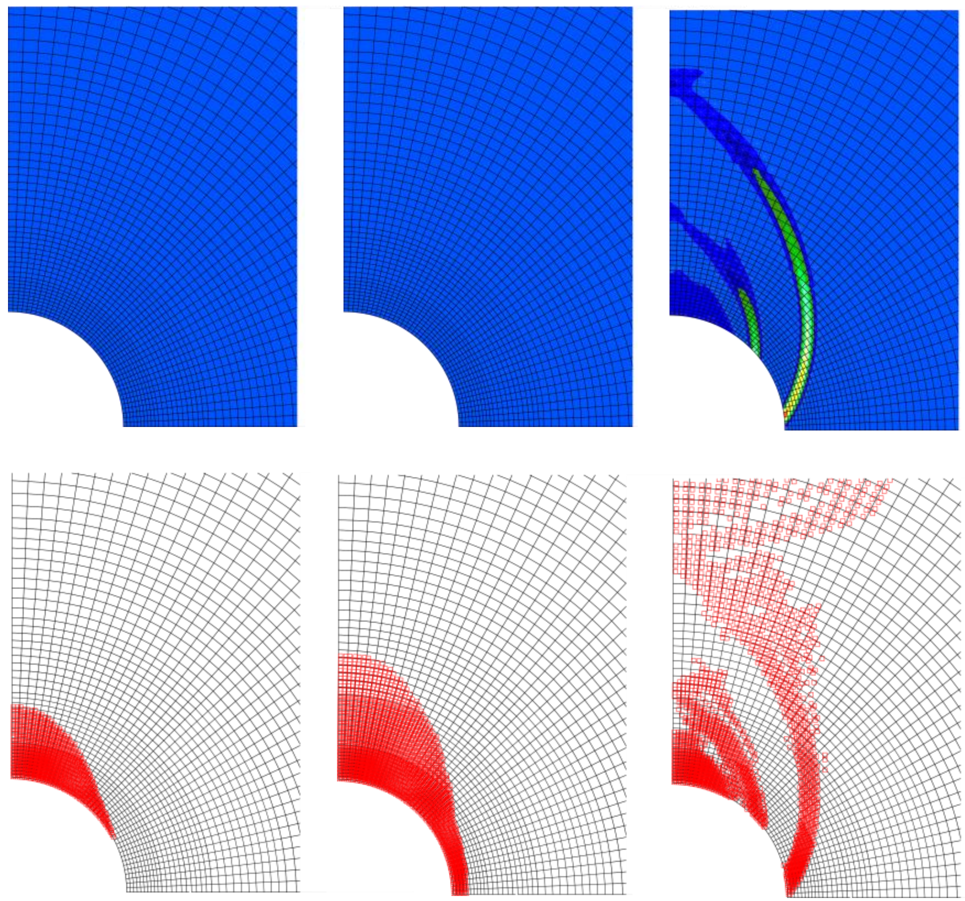

Modelling the EDZ structure

Gallery // to σ_h :

1. Anisotropic stress state + Anisotropic model

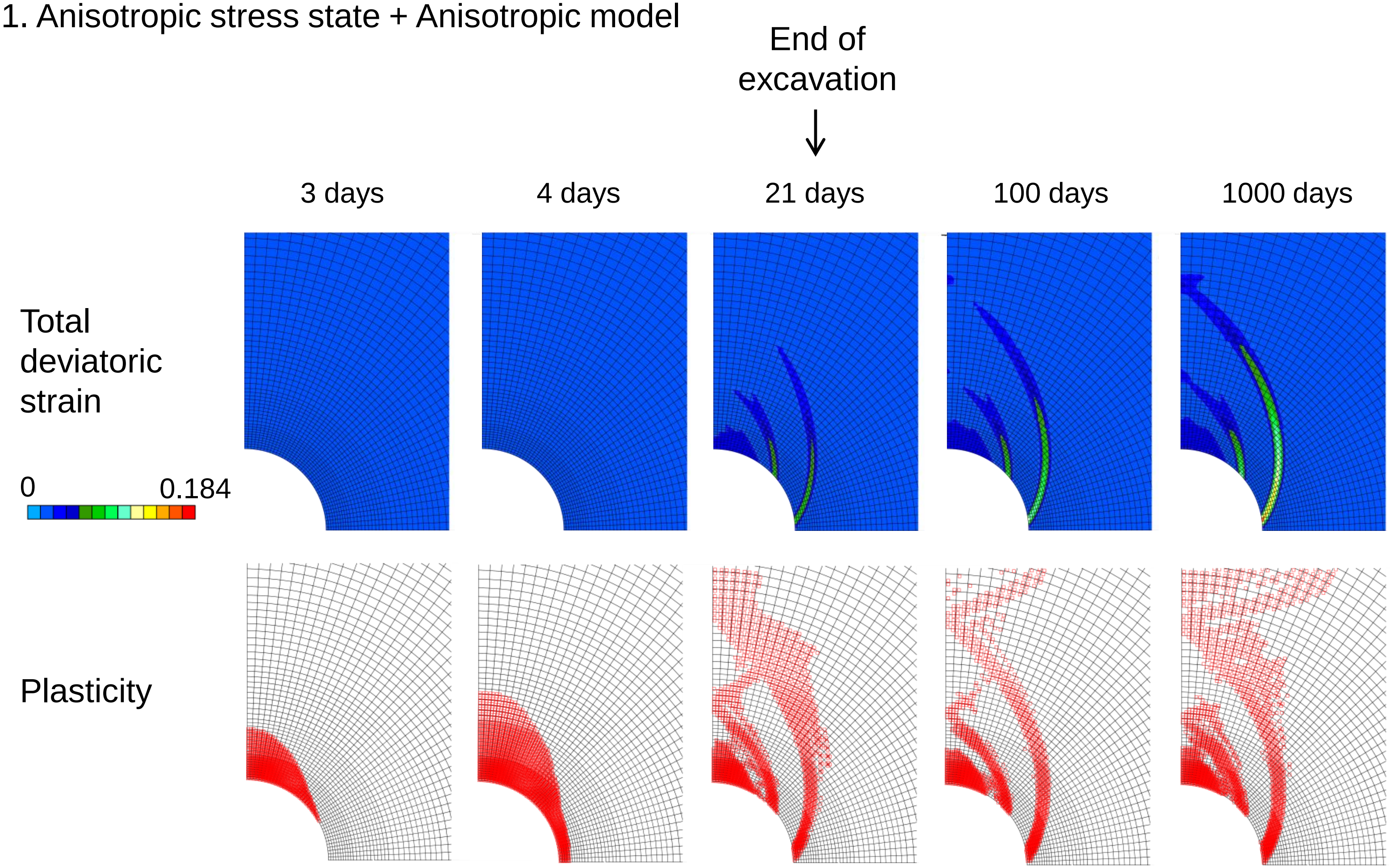

Modelling the EDZ structure

Fractures

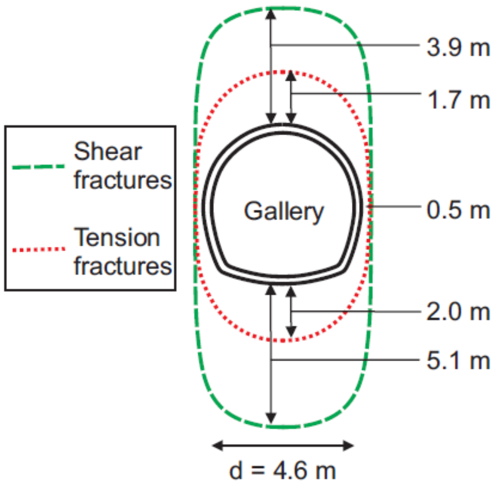

Total deviatoric strain

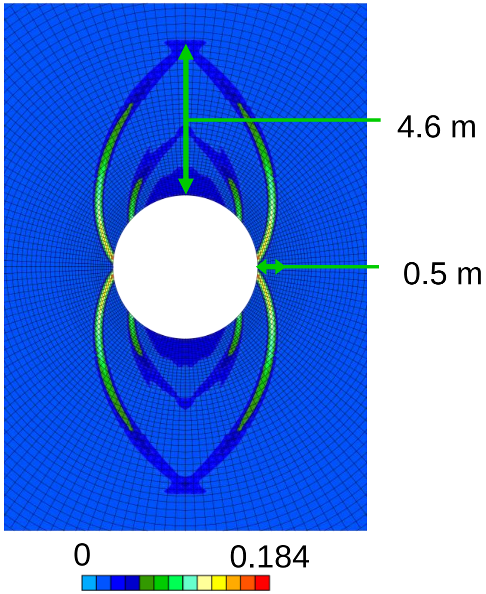

Convergence

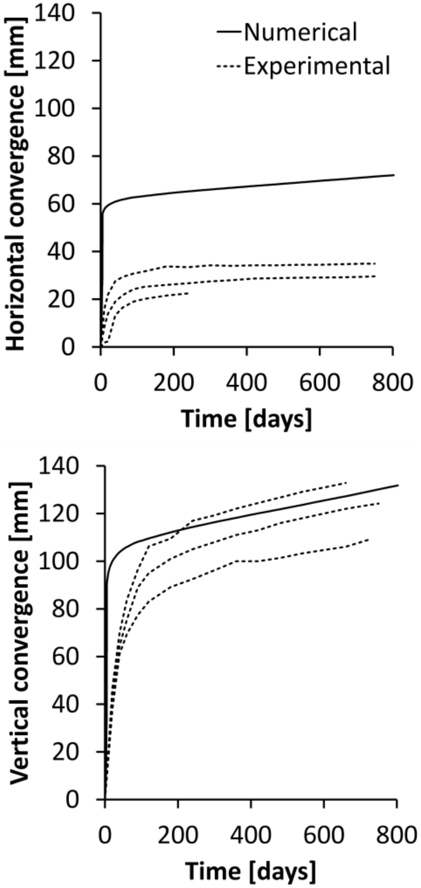

σ anisotropy is the predominant factor leading to strain localisation and to the elliptical shape of the damaged zone.

Modelling the EDZ structure

Gallery // to σ_H :

Isotropic stress state (σ=12 MPa), anisotropic model

HM modelling in 2D plane strain state

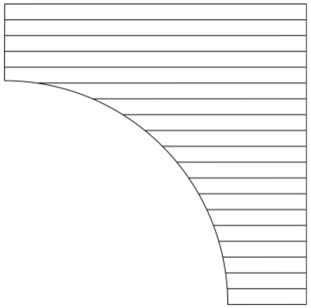

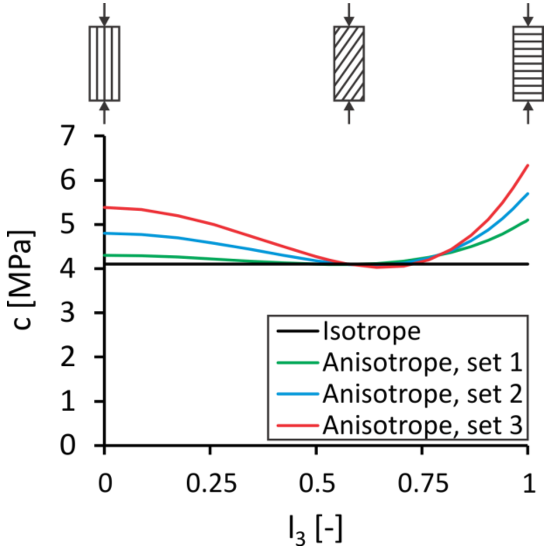

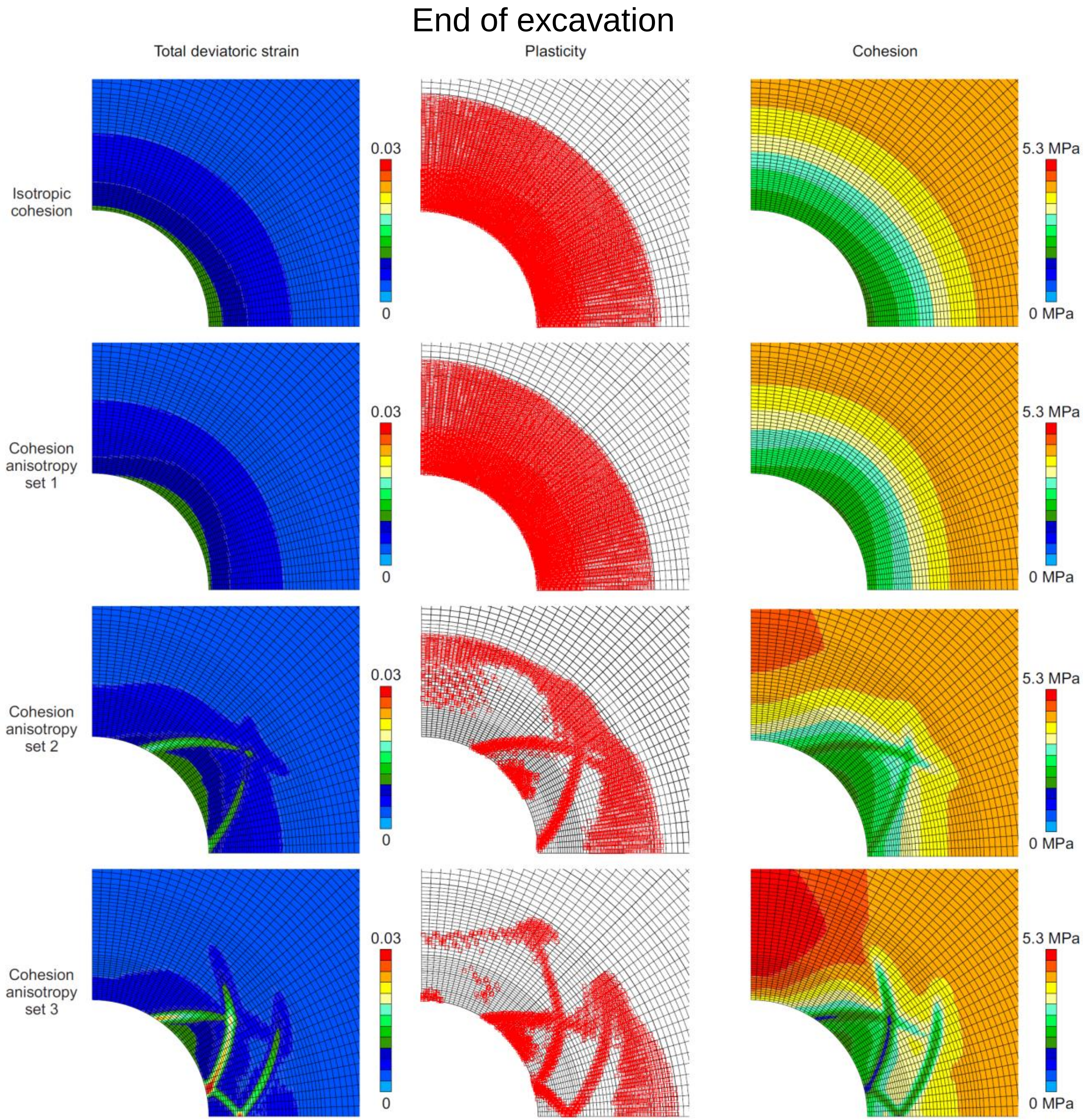

Cohesion evolution :

Anisotropy: $c = a_{ij} l_i l_j = \bar{c}\left(1 + A_{11}(1-3l_2^2) + b_1 A_{11}^2 (1-3l_2^2)^2 + \ldots\right)$ $\quad l_i = \sqrt{\dfrac{\sigma_{i1}^{'2} + \sigma_{i2}^{'2} + \sigma_{i3}^{'2}}{\sigma_{ij}^{'}\sigma_{ij}^{'}}}$

Initially : isotropic σ_{ij} → $c = \bar{c}$ $\quad l_2 = \sqrt{3}/3 = 0.58$

Excavation : $\sigma_r \downarrow$ and $\sigma_{ort} \uparrow$

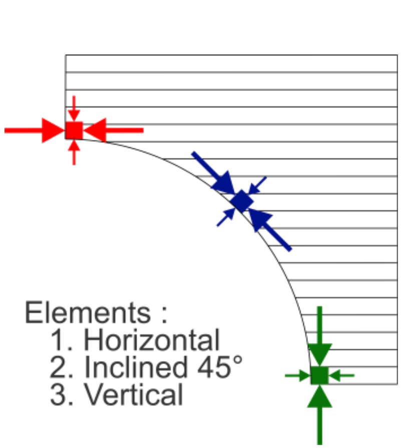

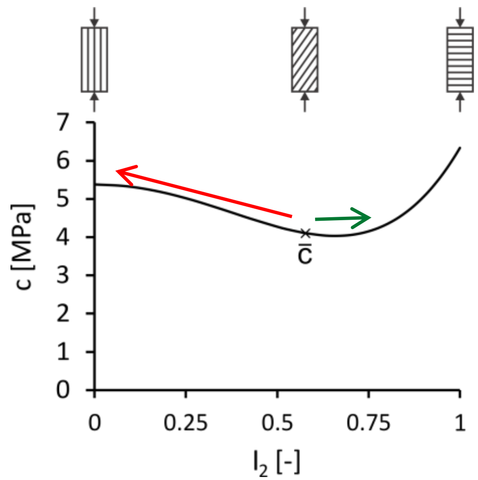

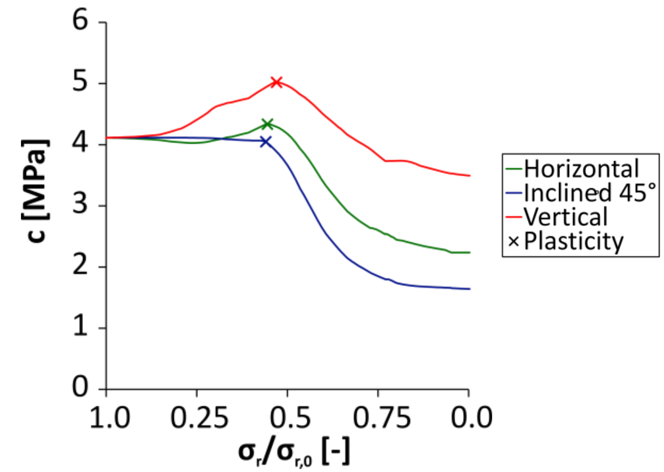

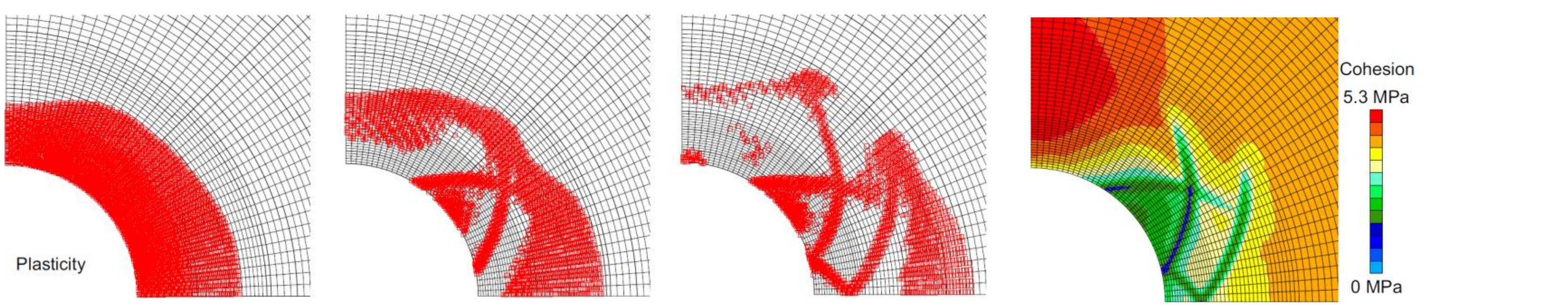

Gallery // to σ_H :

Anisotropic stress state, anisotropic model

$\sigma_{H,0} = 1.3\ \sigma_{v,0} > \sigma_{v,0} = \sigma_{h,0} = 12$ [MPa]

Fractures

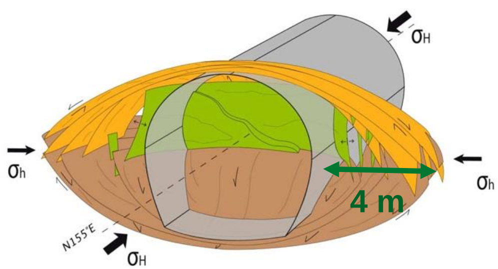

Total deviatoric strain

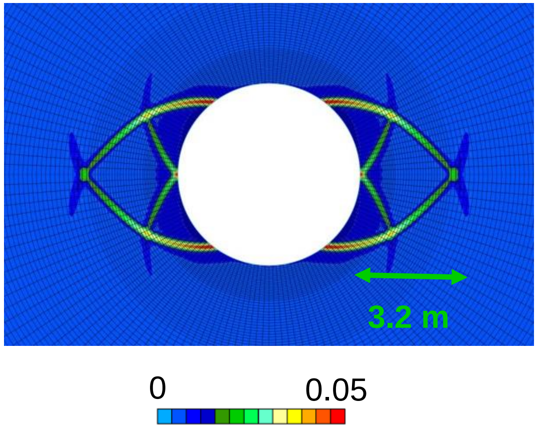

Convergence

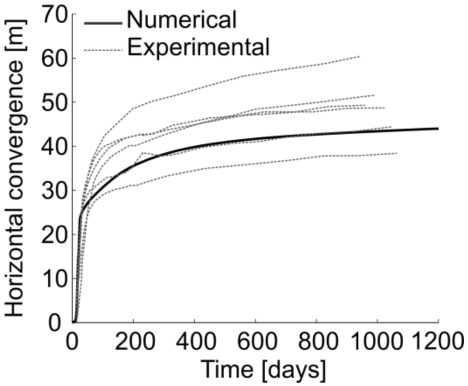

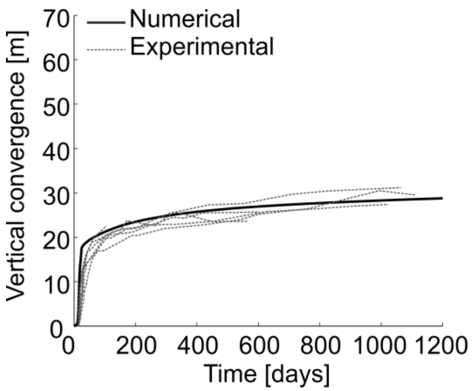

Isotropic stress state in the gallery section does not lead to shear strain localisation unless the material anisotropy is considered.

Material anisotropy seems to be the predominant factor leading to strain localisation and to the elliptical shape of the damaged zone.

Outline

Permeability evolution

In situ evidences :

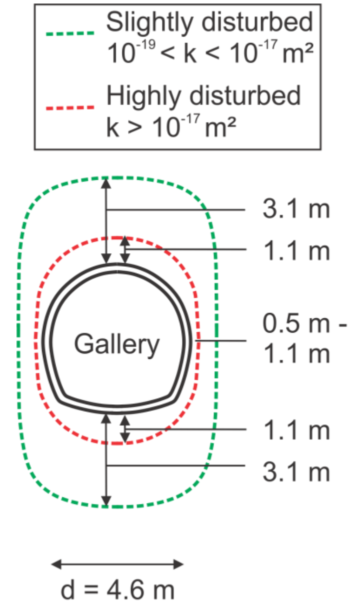

Hydraulic properties are not homogeneous in the damaged zone.

Influence of rock fracturing on intrinsic permeability.

In situ permeability in Callovo-Oxfordian claystone
(Armand et al. 2014, Cruchaudet et al. 2010b)

Permeability variation :

Total deviatoric strain (if $\varepsilon_{eq} > \varepsilon_{eq}^{min}$)

$$\frac{k_{ij}}{k_{ij,0}} = 1 + \alpha(\varepsilon_{eq} - \varepsilon_{eq}^{min})^{\beta}$$

$$\varepsilon_{eq} = \sqrt{\frac{2}{3}\hat{\varepsilon}_{ij}\hat{\varepsilon}_{ij}}$$

$\alpha = 2 \times 10^8$, $\beta = 3$

End of excavation

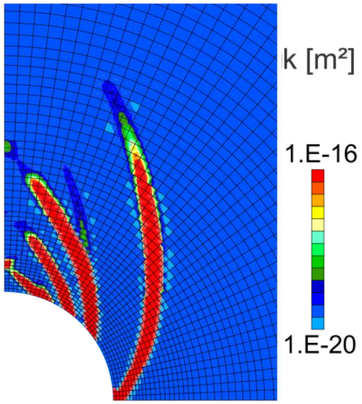

Vertical y-axis

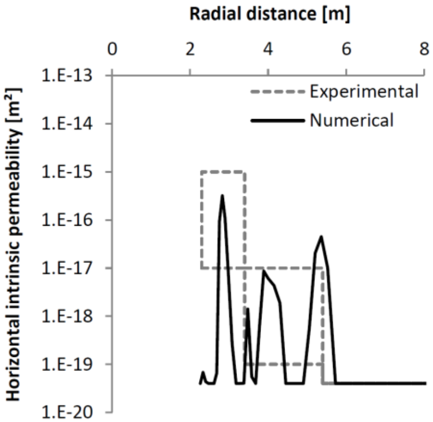

Horizontal x-axis

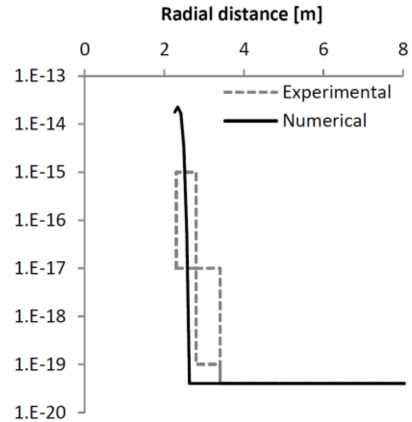

Permeability variation:

$$k_{ij} = k_{ij,0}\left(1 + \beta \left\langle YI - YI^{thr}\right\rangle \hat{\epsilon}_{eq}{}^{3}\right) \qquad YI = \frac{II_{\hat{\sigma}}}{II^{p}_{\hat{\sigma}}}$$

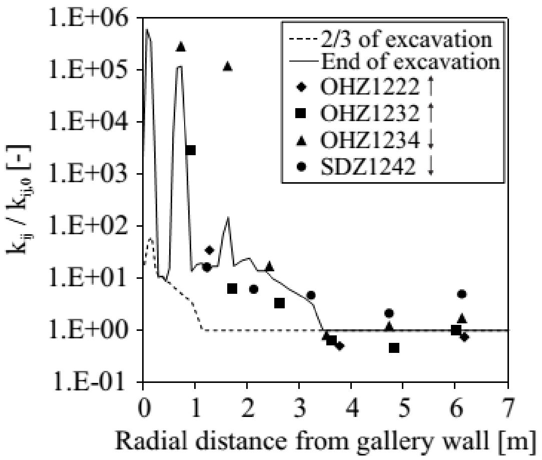

Vertical

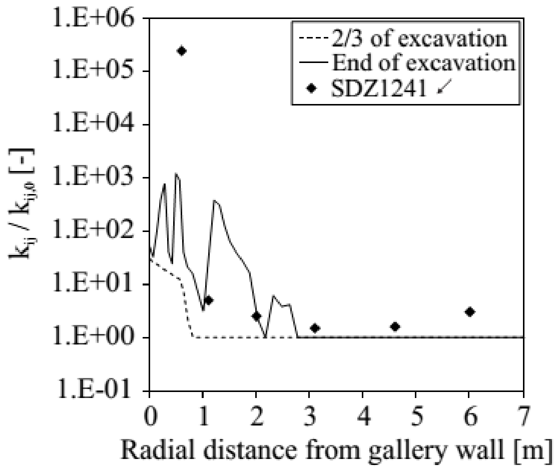

Oblique at 45°

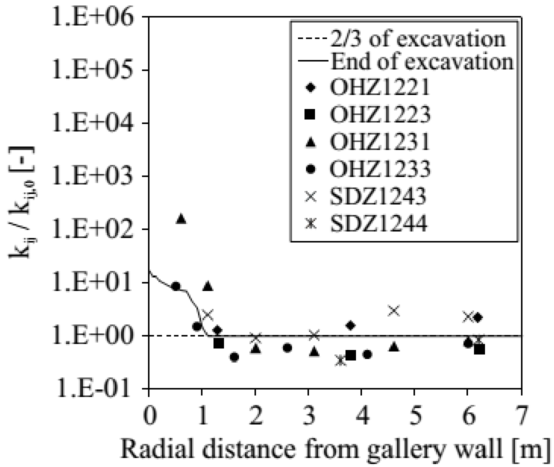

Horizontal

Impact of ventilation:

Two exchange modes can occur at the gallery wall:

- Seepage flow $\begin{cases} \bar{S} = K^{pen}\left(p_w^r - p_{atm}\right)^2 & if\ p_w^r \geq p_w^{cav}\ and\ p_w^r \geq p_{atm} \\ \bar{S} = 0 & if\ p_w^r < p_w^{cav}\ or\ p_w^r < p_{atm} \end{cases}$

- Evaporation flow $\bar{E} = \alpha\left(\rho_v^r - \rho_v^{cav}\right)$

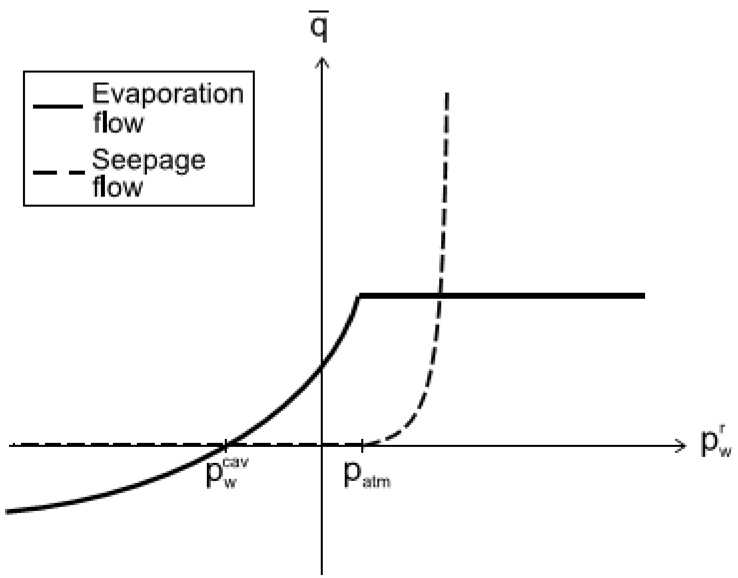

Rock-atmosphere interaction (gallery air ventilation) :

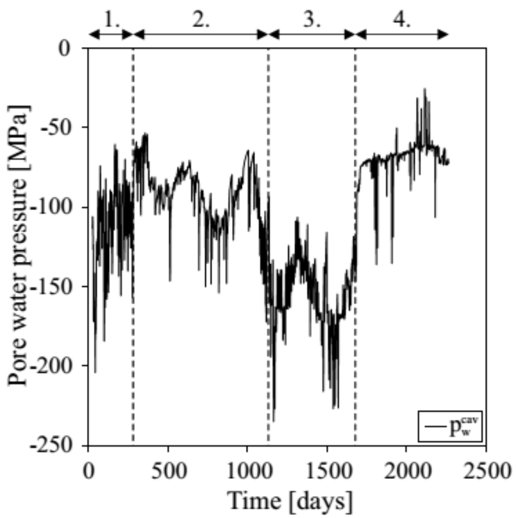

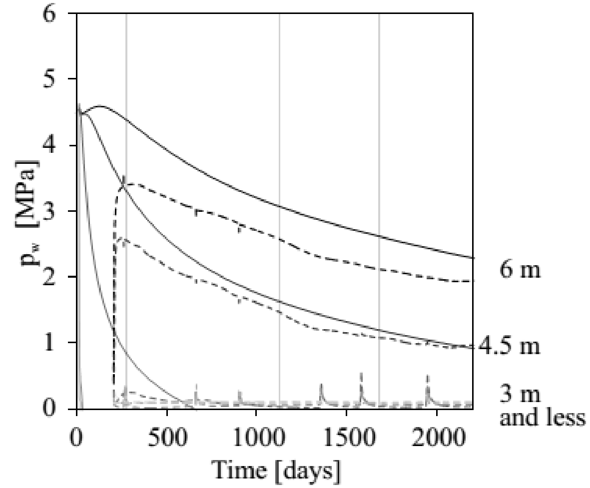

(a) 45°

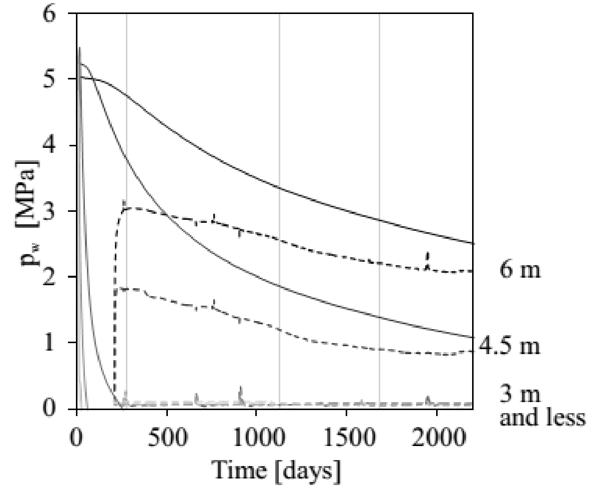

(b) Vertical

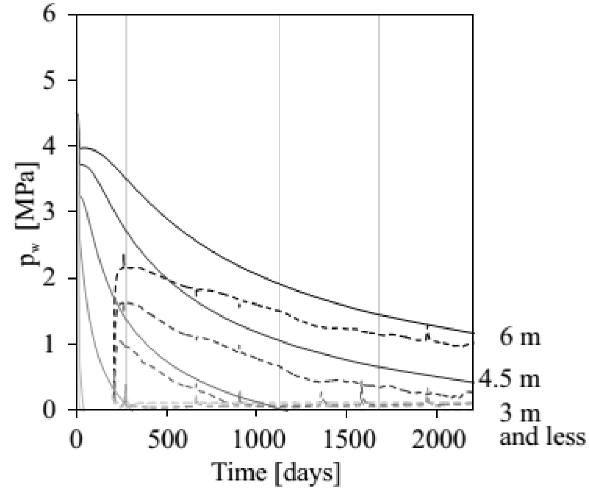

(c) Horizontal

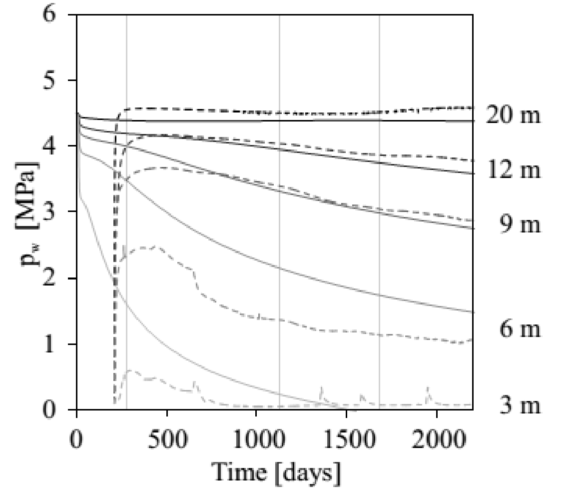

(d) Horizontal

Outline

1. INTRODUCTION
2. SHEAR BAND MODELLING
3. FRACTURES MODELLING
   - GALLERY // TO σ_h
   - GALLERY // TO σ_H
4. PERMEABILITY EVOLUTION
5. CONCLUSION

Conclusions

Damaged zone → strain localisation zone similar to *in situ* measurements

→ modelling provide information about the rock structure and evolution within this zone, as observed *in situ*.

→ rock anisotropy and properties modification

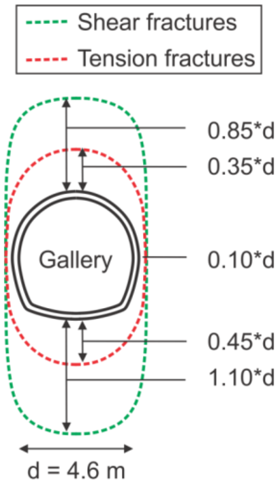

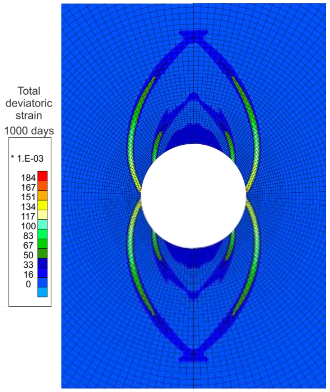

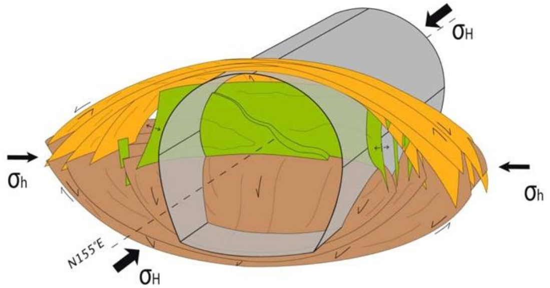

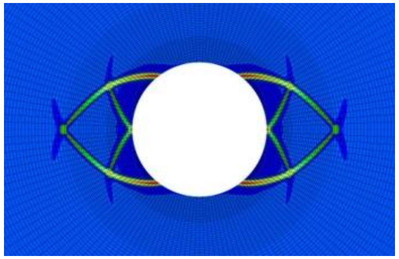

Numerical modelling (LAGAMINE-ULg) :

Mechanical modelling in 3D state.
Classical FE, no second gradient !

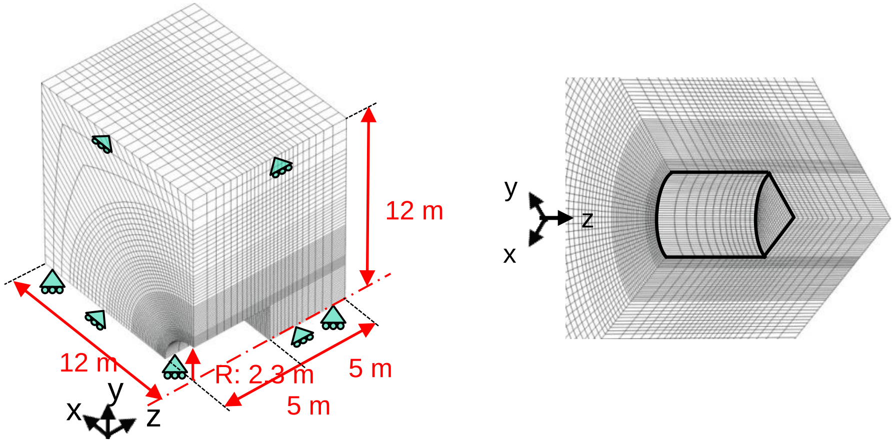

Equivalent deformation ε_{eq} :

ε_{eq} during boring :

3 days	3.25 days	3.5 days	3.75 days	4 days	4.25 days
$\sigma/\sigma_0 = 0.40$	$\sigma/\sigma_0 = 0.35$	$\sigma/\sigma_0 = 0.30$	$\sigma/\sigma_0 = 0.25$	$\sigma/\sigma_0 = 0.20$	$\sigma/\sigma_0 = 0.15$

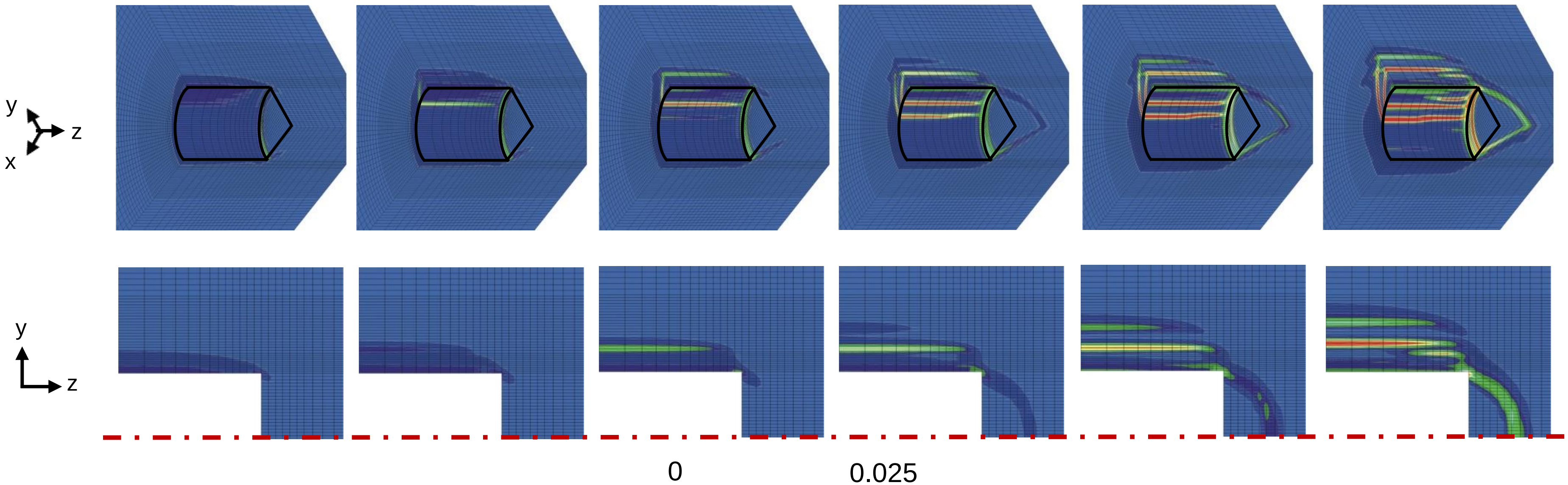

Numerical results for gallery excavation – 3D

Equivalent deformation ε_{eq} :

ε_{eq} for 4.25 days of excavation ($\sigma/\sigma_0 = 0.15$) :

z<0 : excavation zone
z=0 : gallery front
z>0 : rock mass

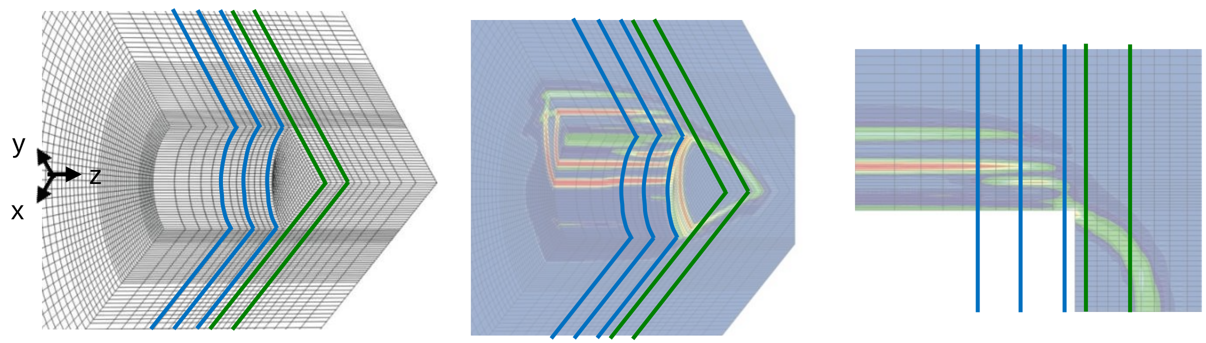

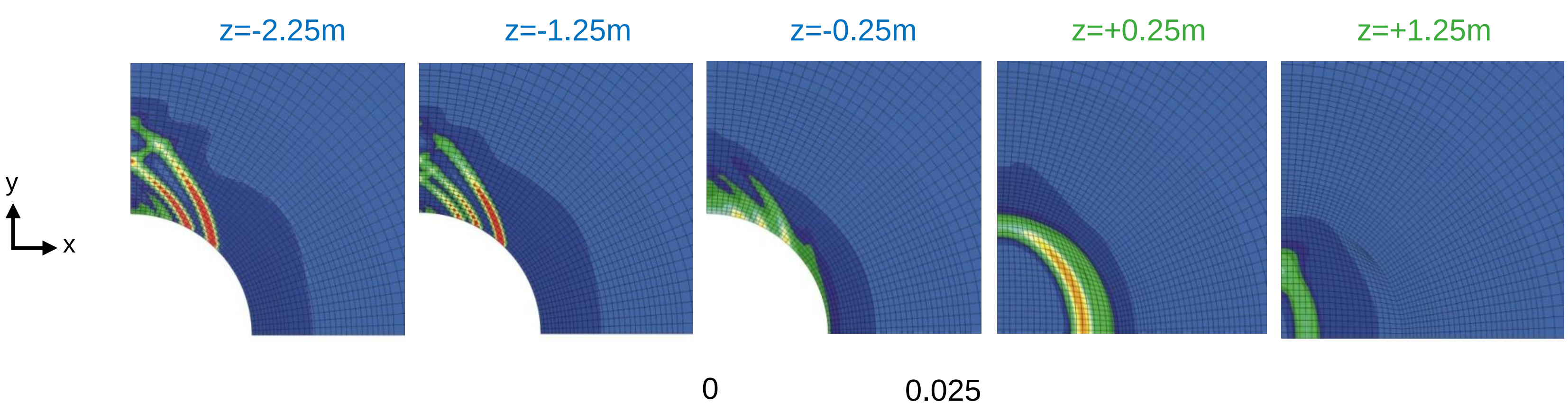

Modelling the EDZ structure

Cross sections :

No ventilation | Ventilation

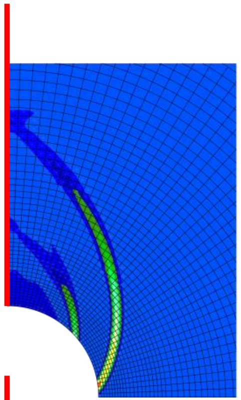

Pore water pressure

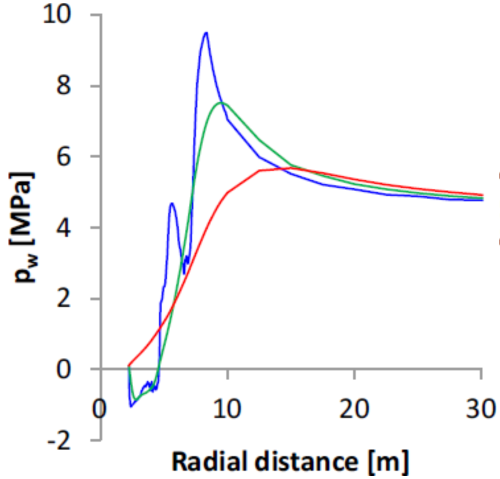

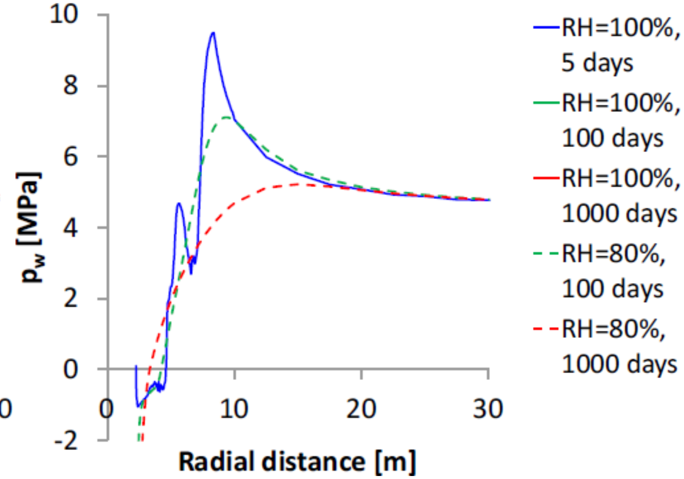

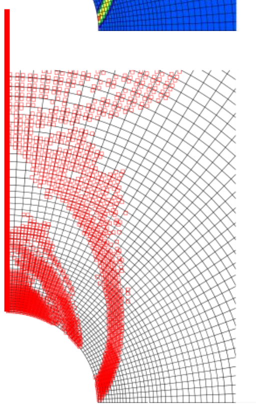

Degree of saturation